



Catalytic hydrodeoxygenation of anisole over Re-MoO_x/TiO₂ and Re-VO_x/TiO₂ catalysts



I.T. Ghompson ^{a,*}, G. Pecchi ^b, J.L.G. Fierro ^c, A. Videla ^d, N. Escalona ^{a,e,f,**}

^a Departamento de Ingeniería Química y Bioprocessos, Escuela de Ingeniería, Pontificia Universidad Católica de Chile, Avenida Vicuña Mackenna 4860, Macul, Santiago, 7820436, Chile

^b Universidad de Concepción, Facultad de Ciencias Químicas, Casilla 160c, Concepción, Chile

^c Instituto de Catálisis y Petroleoquímica, CSIC, Cantoblanco, Madrid, 28049, Spain

^d Departamento de Ingeniería de Minería, Escuela de Ingeniería, Pontificia Universidad Católica de Chile, Santiago, Chile

^e Departamento de Química Física, Facultad de Química, Pontificia Universidad Católica de Chile, Santiago, Chile

^f Centro de Investigación en Nanotecnología y Materiales Avanzados (CIEN-UC), Pontificia Universidad Católica de Chile, Santiago, Chile

ARTICLE INFO

Article history:

Received 7 September 2016

Received in revised form 2 January 2017

Accepted 12 February 2017

Available online 17 February 2017

Keywords:

Hydrodeoxygenation

Anisole

Rhenium

Reducible metal oxides

Molybdenum oxide

Vanadium oxide

ABSTRACT

The hydrodeoxygenation of anisole at 300 °C and 3 MPa H₂ in a batch reactor is used as a model reaction to explore the performance of TiO₂-supported Re-MoO_x and Re-VO_x catalysts. The binary catalysts were prepared with different Re and MoO_x (or VO_x) loadings and characterized by nitrogen physisorption, ICP-MS and AAS, XRD, FTIR, H₂-TPR, NH₃-TPD, H₂-TPD, TEM and XPS techniques. A series of catalysts consisting of a base-metal (Re, Ga, Ni and Co) in combination with reducible metal oxide (Mo and V) were initially screened: due to its oxophilic nature only supported Re catalysts showed the ability to catalyze aromatic C—O bonds to produce aromatic hydrocarbons. This capability was enhanced by pairing Re with partially reduced surface MoO_x (or VO_x) sites, particularly in equimolar proportions. The catalytic activity, expressed as intrinsic reaction rate, was found to rely on the nature of surface Re, Mo and V species: the activity of Re-MoO_x/TiO₂ catalysts is dominated by exposed Mo⁵⁺ sites while that of Re-VO_x/TiO₂ catalysts is controlled by Re⁴⁺ sites. The results also reveal that despite the highest intrinsic activity of Mo⁵⁺ sites, they require the presence of a specific type of active sites such as Re, in appropriate amount, to enable the enhanced benzene/toluene production.

© 2017 Elsevier B.V. All rights reserved.

1. Introduction

Primed by widespread economic and environmental concerns, interests in biomass-derived fuels and chemicals have increased rapidly over the past decade [1]. Pyrolysis of biomass to produce bio-oil represents an attractive alternative to mitigate the dependence on fossil fuels towards relatively lower-carbon sources. However, the full implementation of this process has encountered a variety of hurdles, the most significant of which is the development of effective hydrodeoxygenation (HDO) catalysts to upgrade bio-oil [2]. In that respect, extensive works are being done in developing effective HDO catalysts capable of removing oxygen groups responsible for the low product quality and the instability of bio-oil [1,2].

Lignin derivatives such as guaiacol, anisole and phenol have been used as model compounds to evaluate potential catalysts because they are present in significant quantities in bio-oil [2], in addition to being among the more refractory compounds towards complete oxygen removal [3]. The catalysts include metal sulfides [4,5], noble metals [6–8], non-noble metals [9–13], metal phosphides [14–16], metal carbides [17,18], bifunctional metal/acid catalysts [19–22], among others. However, the development of catalysts with high selective deoxygenation activity and low propensity towards complete hydrogenation of valuable aromatic compounds remains challenging. Since hydrogen efficiency is a vital part of HDO catalysis, there is still the need to improve existing catalysts or develop new catalysts with high specificity to cleaving C—O bonds [22,23].

As reported in the literature, reducible transition metal oxides are among the list of highly selective catalysts for cleaving C—O bonds of phenolic substrates, a list which also includes FeMoP [24], Mo₂C catalysts [17]. The reactivity of reducible metal oxides relies on the formation of surface coordinatively unsaturated sites (CUS) and surface hydroxyl groups through the removal of surface lattice oxygen by reduction [25]: the CUS sites interact with and acti-

* Corresponding author.

** Corresponding author at: Departamento de Ingeniería Química y Bioprocessos, Escuela de Ingeniería, Pontificia Universidad Católica de Chile, Avenida Vicuña Mackenna 4860, Macul, Santiago, 7820436, Chile.

E-mail addresses: isghompson@uc.cl (I.T. Ghompson), neescalona@ing.puc.cl (N. Escalona).

vate O-groups of oxygenated compounds, and the surface hydroxyl groups subsequently donate protons to the chemisorbed substrate, leading to C–O bond scission [26]. Recent studies have demonstrated the ability of partially reduced MoO_3 [27] and ReO_3 [28] catalysts to directly cleave C–O bonds and minimize the complete saturation of C–C bonds in lignin derivatives to obtain aromatic hydrocarbons such as benzene, toluene, and xylene (BTX), important building blocks for downstream petrochemical processing [22,27].

An effective method to further improve the performance of reducible metal oxides is by combining them with other metals in order to create multiple catalytic functions, an essential part of HDO catalysis due to the multiple functional groups present in bio-oil [29]. It has been reported that the interface between the metal and the partially reduced metal oxide modifier can play an important role in C–O bond cleavage [30]: stronger interactions between the O-group in the substrate and the oxide modifier on the surface of the catalyst facilitate hydrogenolysis [29]. Tomishige et al. [29–33] reported that silica-supported Rh– MO_x and Ir– MO_x ($M = \text{Mo}$ and Re) exhibited high activity in selectively dissociating C–O bond in glycerol [31,33], cyclic ethers [29,30] and other substrates [32]. Shimizu et al. [34] found that the co-presence of metallic Ni species and partially reduced MoO_2 was effective in catalyzing the hydrogenation of levulinic acid to γ -valerolactone. Ota et al. [35] attributed the high catalytic performance of ReO_x –Pd/CeO₂ to partially reduced rhenium species. In a recent study, Yang et al. [36] reported that the addition of FeO_x increased the activity, restrained the C–C cleavage and decreased the hydrogen pressure needed for the complete HDO of furanic compounds.

Despite the promising results of the combined metal/metal oxide catalysts for biomass-derived oxygenates, there is a dearth of studies on their application for HDO of phenolic molecules. Hong et al. [37] reported that the high deoxygenation activity of Pd/WO_x/ γ -Al₂O₃ for guaiacol HDO was related to the cooperative function of Pd metal sites and Pd–WO_x acidic sites. Echeandia et al. [38] observed a large enhancement in catalyst performance after Ni incorporation to W⁶⁺ species of activated carbon-supported catalysts, and attributed it to a substantial improvement in surface exposure of the metal oxide species. Nie et al. [39] credited the drastic change in product selectivity upon the addition of Fe to Ni/SiO₂, for the conversion of *m*-cresol, to the presence of oxophilic sites of Fe species which enhanced the deoxygenation activity while inhibiting ring hydrogenation. DFT analysis suggested that stronger interaction between the hydroxyl O and the oxophilic Fe surfaces is responsible for the nearly 4-fold increase in toluene selectivity in comparison to monometallic Ni/SiO₂ catalyst [39]. All these studies have demonstrated the beneficial effect of the combination of elements, providing an incentive to expand the investigation to include other possible metal/metal oxide combinations.

Therefore, the focus of this study is on Re– MO_x /TiO₂ catalysts ($M = \text{Mo}$ or V). The choice of Mo and V oxides is rooted in the existence of cations of multiple stable oxidation states due to the easy conversion of one oxide to another by oxidation and reduction, which is conducive for creating multiple catalytic functionality for HDO reactions [25]. On the other hand, rhenium-based catalysts (ReO_x, ReS₂ and Re metal) have recently been found to be active for the HDO of guaiacol and phenol [28]. Also, Mo, V and Re oxides are among a limited number of metal oxides that possessed both Lewis and Brønsted acid sites [25], making them well-suited as components to prepare metal/metal oxide catalytic functions. TiO₂ was chosen as support because it was found to be more hydrogen efficient than other supports [40]. To the best of our knowledge, Re– MoO_x /TiO₂ and Re– VO_x /TiO₂ catalysts have not been employed for the HDO of lignin model compounds such as anisole which was selected because of the presence of methoxy group, a major functional group of lignin derivatives [22]. Anisole also provides a

useful study of catalytic reaction mechanisms, specifically providing insight into the role of H₂ in the reaction, i.e. whether it is being directed towards the removal of the methyl from the methoxy group, or the direct removal of the whole methoxy group.

In this study, a series of metal/metal oxide catalysts were prepared and screened for the HDO of anisole, after which Re-containing catalysts were selected for structure-activity relationship study aimed at finding the optimum amount of Re and Mo (or V) for the conversion of anisole and selectivity towards aromatic hydrocarbons, setting the stage for developing effective HDO catalysts.

2. Experimental

2.1. Catalyst preparation

A commercial titanium (IV) oxide (TiO₂, $S_{\text{BET}} = 157 \text{ m}^2 \text{ g}^{-1}$, Alfa Aesar), ground and sieved to 100–140 μm , was used as support. The MO_x/TiO_2 ($M = \text{Mo}$, V) samples were prepared by wetness impregnation of TiO₂ with aqueous solution of $(\text{NH}_4)_6\text{Mo}_7\text{O}_{24}\cdot 4\text{H}_2\text{O}$ ($\geq 99.0\%$, Merck) and NH_4VO_3 ($\geq 99.0\%$, Sigma-Aldrich) to give a nominal Mo and V loading of $0.88 \text{ mmol g}_{\text{cat}}^{-1}$ (corresponding to 7.2 mol%). After impregnation, the samples were kept at room temperature for 24 h, and then evaporated to dryness at 50 °C under vacuum using a rotary evaporator. The samples were further dried at 110 °C for 15 h, and calcined at 500 °C (ramp rate of 2 °C min⁻¹) for 4 h.

The $\text{M}_A\text{-MO}_x/\text{TiO}_2$ ($\text{M}_A = \text{Re}$, Ga, Ni, Co; $M = \text{Mo}$, V) catalysts were prepared by wetness impregnation of calcined MO_x/TiO_2 samples with aqueous solution of NH_4ReO_4 ($\geq 99.0\%$, Sigma-Aldrich), $\text{Ga}(\text{NO}_3)_3\cdot x\text{H}_2\text{O}$ (99.9%, Sigma-Aldrich), $\text{Ni}(\text{NO}_3)_2\cdot 6\text{H}_2\text{O}$ ($>99\%$, Merck) and $\text{Co}(\text{NO}_3)_2\cdot 6\text{H}_2\text{O}$ ($>99\%$, Merck) to give a nominal M_A loading of $0.34 \text{ mmol g}_{\text{cat}}^{-1}$, and was followed by the same drying procedures described above. All the catalysts, except the Re– MO_x/TiO_2 catalysts, were calcined at 500 °C (ramp rate of 2 °C min⁻¹) for 4 h. The Re-containing samples were calcined at 300 °C for 0.5 h.

The M_A/TiO_2 ($\text{M}_A = \text{Re}$, Ga, Ni, Co) series were prepared by wetness impregnation of TiO₂ support with aqueous solution of NH_4ReO_4 , $\text{Ga}(\text{NO}_3)_3\cdot x\text{H}_2\text{O}$, $\text{Ni}(\text{NO}_3)_2\cdot 6\text{H}_2\text{O}$ and $\text{Co}(\text{NO}_3)_2\cdot 6\text{H}_2\text{O}$ to give a nominal M^I loading of $0.34 \text{ mmol g}_{\text{cat}}^{-1}$ (corresponding to 2.7 mol%), and was followed by the same drying and calcination procedures described previously.

A series of Re– MO_x/TiO_2 ($M = \text{Mo}$, V) catalysts were prepared by sequential wet impregnation by varying the Re and Mo (or V) loadings, using the same method and conditions previously described for Re-containing samples. The catalysts prepared are represented as $X\text{Re YMo}$ and $X\text{Re YV}$, where X and Y denote the theoretical mole percentage of Re and Mo (or V), respectively, i.e. $X = \text{Re}/(\text{M} + \text{Re})$ and $Y = \text{M}/(\text{M} + \text{Re})$. Data for the following catalysts are reported in this paper: 100Re, 100Mo, 100V, 30Re70Mo, 50Re50Mo, 70Re30Mo, 30Re70V, 50Re50V and 70Re30V.

The calcined samples were reduced *ex situ* under a flow of H₂ (60 mL min⁻¹) at 500 °C (ramp rate of 10 °C min⁻¹) for 3 h. The samples were cooled down to ambient temperature under N₂ (60 mL min⁻¹), and then passivated with 5% O₂/N₂ (30 mL min⁻¹) for 1 h with the reactor immersed in an isopropanol/liquid nitrogen slurry bath. Passivation was continued for 1.5 h at ambient temperature.

2.2. Catalyst characterization

Molybdenum and vanadium contents of the calcined catalysts were determined by AAS (using a Perkin Elmer AAnalyst 100 AA Spectrometer), while rhenium metal loading was determined by

ICP-MS (using a PerkinElmer Elan 9000 ICP Mass Spectrometer). The samples were digested in a microwave digester using concentrated HNO₃ acid prior to ICP-MS analysis and a mixture of HNO₃, HF and H₂O₂ prior to AAS analyses.

Nitrogen adsorption-desorption isotherms of the support and calcined catalysts were obtained at -196 °C using a Micromeritics TriStar II 3020 instrument. Prior to the measurements, the samples were degassed under vacuum at 200 °C for 3 h in a nitrogen flow. The BET specific surface area was calculated from the adsorption branch of the isotherms in the range 0.05 ≤ P/P₀ ≤ 0.25 and the total pore volume was recorded at P/P₀ = 0.99. The average pore diameter was estimated via the desorption branch using the BJH method.

X-ray Diffraction (XRD) patterns of the support and the reduced-passivated catalysts were obtained using a Rigaku diffractometer equipped with a Ni-filtered CuKα₁ radiation ($\lambda = 1.5418 \text{ \AA}$). The standard scan parameters were 10–90° 2θ with a step size of 0.02° 2θ and a counting time of 0.4 s per step. Identification of the phases was achieved by reference to ICDD files.

Transmission Electron Microscopy (TEM) measurements of selected catalysts were carried out with a JOEL JEM-1200 EX II electron microscope operating at 120 kV. The samples were ground and dispersed in 50% ethanol in H₂O solution and electrostatically mounted onto carbon-coated grids.

FTIR spectroscopy analyses of the support and selected calcined samples were performed on a Nicolet Nexus FTIR in the wavenumber range (4000–400 cm⁻¹) and with a scan of 64. The samples were prepared using a 1:100 mg of catalysts and KBr support.

H₂-Temperature Programmed Reduction (TPR) of the calcined catalysts was performed using a TPR/TPD 2900 Micromeritics instrument fitted with a thermal conductivity detector (TCD). Before the measurements, 50 mg of catalyst was loaded in a U-shaped quartz reactor and dried in flowing He (50 mL min⁻¹) at 110 °C for 0.5 h to remove any weakly retained moisture. Subsequently, H₂-TPR was performed from 50 °C to 900 °C at a heating rate of 10 °C min⁻¹ in a stream of 5% H₂/Ar (50 mL min⁻¹, certified mixture grade, Linde). The effluent gas was passed through a cold trap filled with a mixture of isopropanol and liquid nitrogen to remove water vapor before entering the TCD detector. The amount of H₂ consumed per gram of catalyst sample was calculated from integral of the area under the TCD signal previously calibrated by the reduction of CuO (Micromeritics) as reference.

H₂-Temperature-Programmed Desorption (TPD) of selected catalysts was performed in the same apparatus as the H₂-TPR experiment. The sample (50 mg) was first dried under He at 110 °C for 0.5 h, reduced under H₂ (50 mL min⁻¹) at 500 °C for 3 h, and cooled to 50 °C under He. The sample was swept with He to restore the TCD baseline. H₂-TPD was performed at a heating rate of 10 °C min⁻¹ up to 800 °C in flowing He (50 mL min⁻¹).

The acidity of the catalysts was determined by Temperature-Programmed Desorption of ammonia (TPD-NH₃) using the same apparatus described for TPR. The sample was first dried under He (50 mL min⁻¹) at 110 °C for 0.5 h, reduced under H₂ (50 mL min⁻¹) at 500 °C for 3 h, and cooled to 110 °C under He. The sample was then saturated with NH₃ using He (50 mL min⁻¹) as a carrier gas, purged with He for 0.5 h to remove physisorbed NH₃, and subsequently cooled to ambient temperature under He. Once the TCD baseline was restored, NH₃-TPD was performed at a heating rate of 10 °C min⁻¹ up to 850 °C in flowing He (50 mL min⁻¹). The amount of NH₃ desorbed per gram of catalyst was calculated from ammonia mean calibrated areas and ammonia TPD analytical areas.

X-ray Photoelectron Spectroscopy (XPS) measurements were recorded on a VG Escalab 200R electron spectrometer fitted with a Mg K α (1253.6 eV) photon source. The reduced-passivated catalysts were pre-reduced *in situ* at 300 °C to remove the passivation layer. The binding energies (BE) were referenced to the C 1s level at 284.8 eV. An estimated error of ±0.1 eV can be assumed for all

measurements. Intensities of the peaks were calculated from the respective peak areas after background subtraction and spectrum fitting by the standard computer based statistical analysis which included fitting the experimental spectra to a sum of Gaussian and Lorentzian lines (90G-10L) using a least squares minimization procedure for χ^2 with the help of the XPS peak software. Relative surface atomic ratios were determined from the corresponding peak areas, corrected with tabulated sensitivity factors [41], with a precision of 7%.

2.3. Catalyst testing

The passivated catalysts were evaluated for anisole hydrodeoxygenation in a 300 mL stirred-batch autoclave set-up (Parr Model 4841) at 300 °C and under a hydrogen pressure of 3 MPa for 4 h. The liquid reactant consists of 2.07 mL anisole (99%, Merck) dissolved in 80 mL dodecane (as solvent, 99%, Merck), while 700 μL of hexadecane (99%, Merck) was added as an internal standard. 200 mg of catalyst was added to the liquid mixture in the reactor, purged with a continuous flow of nitrogen (99.995%, Linde) for 20 min to evacuate air from the system, heated to 300 °C while stirring at 700 rpm, and charged with hydrogen (99.995%, Linde) to 3 MPa. The start of the reaction was assumed to be when the reaction temperature was reached and H₂ was introduced into the reactor. The reaction was punctuated by the addition of hydrogen to maintain the pressure for the entire duration of the experiment. Aliquot of 0.5 mL was periodically withdrawn during the course of the reaction and identified by a Perkin Elmer GCMS-SQ8T GC (Clarus 680) equipped with an Elite-1 column (Perkin Elmer, 30 m × 0.32 mm, film thickness of 0.25 μm). The liquid samples were quantified by a Perkin Elmer GC (Clarus 400) also equipped with an Elite-1 column and a FID. The reactant and products were also identified by their column retention time in comparison with available standards.

The conversion of anisole (X_{ANI}) was calculated from:

$$X_{ANI} (\%) = \frac{n_{anisole}^0 - n_{anisole}^i}{n_{anisole}^0} \times 100 \quad (1)$$

where $n_{anisole}^0$ is the initial moles of anisole in the solution (mol) and $n_{anisole}^i$ is the moles of anisole at time i (mol). The initial reaction rate r_s (mol g⁻¹ s⁻¹) was calculated from the initial slope of the conversion vs. time plot b (s⁻¹) and the mass of the catalyst m (g) according to (Eq. (2)):

$$r_s = \frac{b \times n_{anisole}^0}{m} \quad (2)$$

The product selectivity was calculated from:

$$\text{Selectivity} (\%) = \frac{n_{productj}}{n_{anisole \text{ converted}}} \times 100 \quad (3)$$

where $n_{productj}$ is the moles of product j (mol) and $n_{anisole \text{ converted}}$ is the moles of anisole converted (10%).

Repeated runs at the same conditions were performed to ensure satisfactory reproducibility of the data.

3. Results and discussion

3.1. Screening of catalysts

Conversion of anisole was used to screen a series of metal/metal oxide catalysts under batch conditions at 300 °C and 3 MPa H₂. The reaction scheme is depicted by Fig. 1, whereby anisole proceeds either through (1) demethylation (DME) of O—CH₃ to form phenol, (2) or demethoxylation (DMO) of C_{aromatic}—OCH₃ to form benzene, (3) or methyl transfer (MT) of some residual methyl groups from DME of anisole on the catalyst surface to form cresols [22]. Benzene

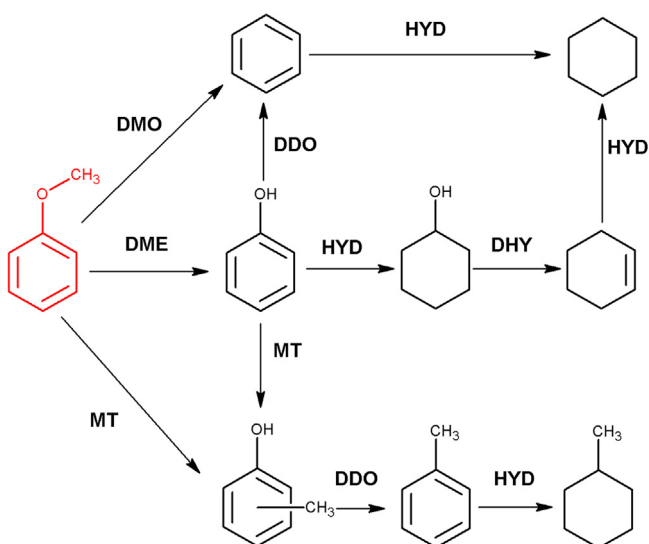


Fig. 1. Reaction scheme for the conversion of anisole, adapted from Saidi et al. [1], showing demethylation (DME), demethoxylation (DMO), methyl-transfer (MT), hydrogenation (HYD), direct deoxygenation (DDO) and dehydration (DHY) reactions.

can also be produced from phenol through direct deoxygenation (DDO). It has been reported that DDO is unlikely to occur due to the high bond dissociation energy (BDE) of the C_{aromatic}—OH bond in phenolic compounds (i.e. 74 kJ mol⁻¹ higher than the BDE

of C_{aromatic}—OCH₃ bond) [3,22]; however, TiO₂-supported catalysts have recently been reported to exhibit a tendency towards direct C—O bond cleavage due to its ability to accept and donate a proton [42–44]. Phenol can also be converted via sequential ring hydrogenation-dehydration (HYD-DHY) route to form cyclohexanol, and subsequently cyclohexene. Cyclohexane can be produced from hydrogenation of cyclohexene and benzene. Along the other pathway, hydrodeoxygenation of cresols forms toluene, which can undergo a final hydrogenation step to form methylcyclohexane.

Fig. 2 illustrates the performance of the screened catalysts. Initial reaction rates ($\times 10^{-6}$ mol_{anisole} g_{cat}⁻¹ s⁻¹) are given in **Fig. 2a**. The Re-containing catalyst was the most active among all the catalyst series, indicating a higher reactivity of Re surface species compared to Ni, Ga and Co. The M_A-MoO_x/TiO₂ catalysts were more active than its monometallic counterpart, attributed to the combined effect of the presence of MoO_x species which enhances the activations of the O-group of anisole and the metallic centers responsible for hydrogen activation and donation [29,45]. In contrast, the effect of VO_x on the initial reaction rate was negligible or slightly negative, suggesting that either VO_x sites is inactive or that M_A is the more dominant sites on the M_A-VO_x/TiO₂ catalysts. Aqsha et al. [46] similarly reported that Mo-promoted Ni/TiO₂ catalyst was more active than its V-promoted one during the HDO of guaiacol due, in part, to its higher acidity.

Products distribution (**Fig. 2b**) was calculated at anisole isoconversion (10%) in order to perform quantitative comparison of intrinsic selectivity. The M_A/TiO₂ series showed selectivity to phenol above 50%, lower amount of cresols and cyclohexane, and traces

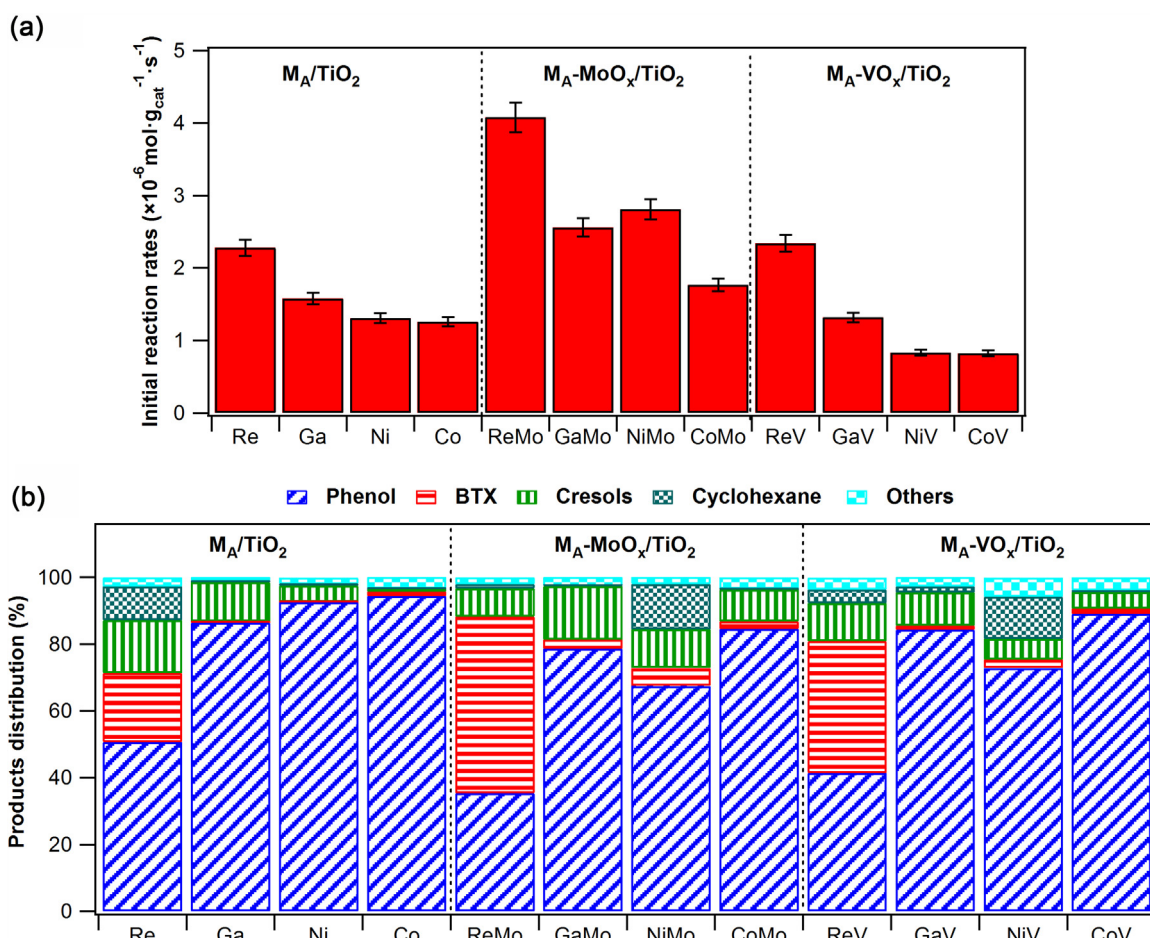


Fig. 2. (a) The initial reaction rates and (b) products distribution calculated at 10% anisole conversion over a series of metal/metal oxide catalysts. Reaction conditions: anisole (19.04 mmol), catalyst (200 mg), dodecane (80 mL), 300 °C, 3 MPa H₂, 4 h.

of methanol, cyclohexanol, cyclohexene and methylcyclohexane (Fig. 2b). The most notable result is the 19% selectivity to aromatics (benzene, toluene and xylene; BTX) obtained over Re/TiO₂. The selectivity of the other series also shows substantially higher BTX with the Re-based catalysts. The results also show that the presence of MoO_x and VO_x enhanced selectivity to BTX by 60% and 48%, respectively (compared to Re/TiO₂). Based on the reaction scheme in Fig. 1, DME of anisole to phenol is the most dominant route of primary conversion, and the thermodynamically favorable pathway: for example, BDE of O—CH₃ bond is 164.4 kJ mol⁻¹ lower than the BDE of C_{aromatic}—OCH₃ bond [3]. However, the Re-containing catalysts exhibited a capability to directly cleave the C—O bond in anisole and/or phenol because Re is strongly oxophilic with a higher propensity for interacting with oxygen, quite different from Ni, Co and Ga [39,47]. This assessment becomes even more apparent when one considers the effect of the presence of MoO_x and VO_x sites on benzene selectivity. Typically, the co-existence of metallic sites and oxygen vacancy sites of lower oxidation state metal oxides facilitates C—O bond cleavage: the oxygen vacancy sites aid in the adsorption and activation of anisole while the metallic sites dissociates hydrogen which then attacks the adsorbed phenoxide ion, leading to rupture of the C—O bond. However, Fig. 2b shows that the combination of MoO_x or VO_x species with Ga, Ni and Co species barely altered the selectivity behavior in comparison to the monometallic catalysts, illustrating the unique attribute of Re in its ability for C—O bond cleavage, in accordance with our previous results [28,48].

In light of these results which demonstrate that Re-containing catalysts clearly stand out for its ability to cleave C—O bonds in anisole and phenol, they were selected for further studies to determine the optimized Re/MoO_x and Re/VO_x compositions. Characterizations by XRD, FTIR spectroscopy, TPR, NH₃-TPD, TEM, H₂-TPD, XPS were performed to delineate the bulk and surface properties of these TiO₂-supported Re-MoO_x (or VO_x) catalysts.

3.2. Characterization of Re-MoO_x/TiO₂ catalysts

The elemental analysis of the calcined catalysts determined from ICP-MS and AAS analyses is reported in Table 1. The Re, Mo and V contents agree well with the nominal loadings.

The BET specific surface area (S_{BET}), total pore volume (V_p) and average pore diameter (d_p) of the support and catalysts are also listed in Table 1. As expected, all the catalysts possessed lower S_{BET} and V_p compared to the support, indicating partial blockage of the support's porous structure. The S_{BET} of the molybdenum-based catalysts ranged from 67 to 130 m² g⁻¹ while the vanadium-based catalysts ranged from 47 to 74 m² g⁻¹. The VO_x-based catalysts have lower surface areas than their comparable MoO_x-based counterparts, suggesting preferential deposition of vanadium oxides species in the pores which reduced the accessible porosity.

XRD patterns of the support and passivated catalysts are displayed in Fig. 3. All the samples showed diffraction peaks corresponding only to the anatase phase of TiO₂ (01-086-1157), implying that transition to the rutile polymorph of TiO₂ did not occur. However, no crystalline MoO_x and VO_x peaks were detected which is indicative of dispersion below the theoretical monolayer surface coverage of TiO₂-supported catalysts, or that the catalysts contained small crystallites below the detection limit [49]. Furthermore, no appreciable shifts in the (101) anatase peak were observed, indicating that Mo or V were not incorporated into the TiO₂ lattice. This is not unexpected since the ionic radius of Mo⁶⁺ and V⁵⁺ are almost comparable to that of Ti⁴⁺ [50]. However, there was a slight shift observed for the 100Re catalyst, probably due to Re-induced modification of the TiO₂ lattice during reduction. The diffraction patterns of Re-MoO_x/TiO₂ and Re-VO_x/TiO₂ catalysts show weak peaks at $2\theta = 40.4^\circ$ and 42.8° indexed as Re metal

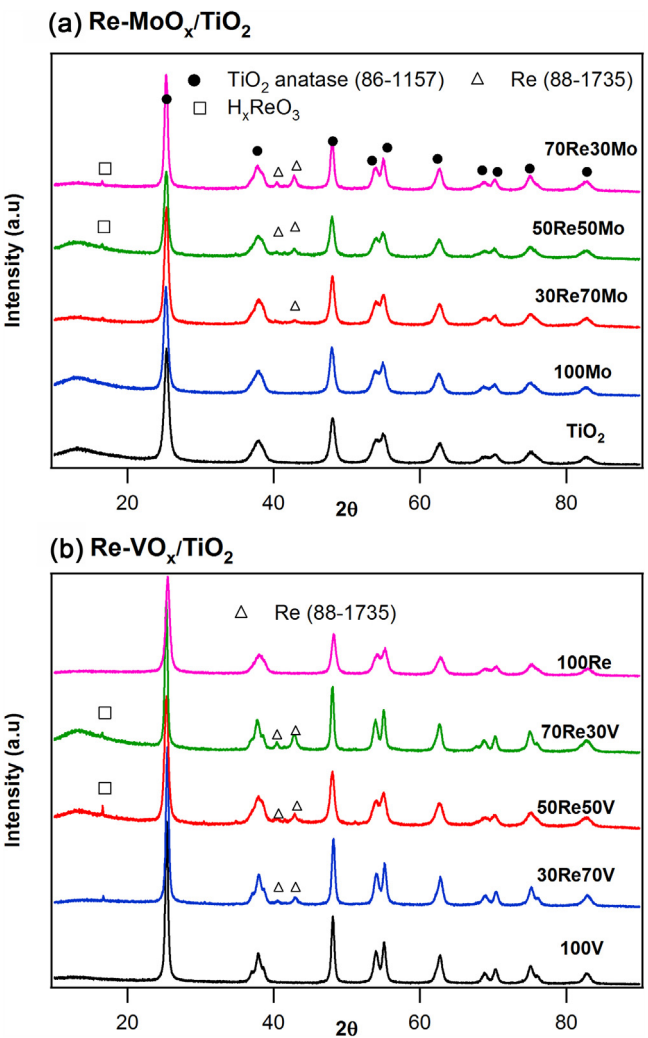


Fig. 3. XRD patterns of passivated-reduced Re-based catalysts. Reduction conditions: 60 mL min⁻¹ H₂, heating rate 10 °C min⁻¹, 500 °C, 3 h. Passivation conditions: 30 mL min⁻¹ 5% O₂/N₂, 2.5 h.

(01-071-6589). A peak at 16.5° 2θ is assigned to H_xReO₃ bronze derived from insertion of atomic hydrogen, similar to that reported in the literature [51,52]. The Re metal average crystallite size (nm) was estimated from the Scherrer equation [53] using the Re (101) diffraction ($2\theta = 42.8^\circ$) for catalysts with discernible peaks. The instrumental contribution to line broadening was accounted for by measuring a silicon standard (NIST SRM 640e) using an identical optical configuration. The Re metal crystallite size in the catalysts were similar (12–16 nm), suggesting that it was not influenced by changing Re and Mo (or V) compositions within the range of loading used. It should be noted that CO/H₂ chemisorption measurement was not performed because it has been reported that the presence of metal oxide species hinders chemisorption and accordingly it overestimates the calculated particle size [37,54].

TEM images of a selection of catalysts are shown in Fig. 4. The images of the 100Mo (Fig. 4a) and 100V catalysts (Fig. 4b) show dark and white fields with regular and well-formed morphology of TiO₂ nanocrystals. The particles are in the size range of 9–11 nm which is in agreement with the average crystalline diameter of 11 nm calculated using Scherer equation of the (101) anatase peak. The contrast between the oxidic Mo or V components and the support is not sufficiently clear to allow the distinction of the morphology of MoO_x or VO_x particles. Conversely, TEM images of the Re-containing catalysts – 100Re (Fig. 4c), 30Re70Mo (Fig. 4d) and 30Re70V (Fig. 4e)

Table 1

Nitrogen adsorption-desorption and elemental analysis results of calcined catalysts.

Samples	Elemental content (wt%)				$\left(\frac{M}{M+Re}\right) \times 100$	S_{BET} ($m^2 g^{-1}$)	V_p ($cm^3 g^{-1}$)	d_p (nm)				
	Mo or V		Re									
	Nominal	Real	Nominal	Real								
TiO ₂	–	–	–	–	–	157	0.32	8.2				
100Mo	8.5	8.6	–	–	100	130	0.26	8.0				
30Re70Mo	8.5	9.4	6.3	5.0	78	115	0.26	8.1				
50Re50Mo	5.6	5.5	10.8	9.3	53	103	0.24	8.2				
70Re30Mo	3.2	3.2	15.2	12.9	33	67	0.21	11.7				
100Re	–	–	6.3	5.6	0	144	0.32	8.2				
100V	4.7	4.5	–	–	100	74	0.22	14.3				
30Re70V	4.7	4.8	6.6	5.5	77	69	0.22	14.2				
50Re50V	3.1	3.0	11.1	9.1	55	63	0.22	12.3				
70Re30V	1.7	1.2	16.0	12.6	26	47	0.19	16.2				

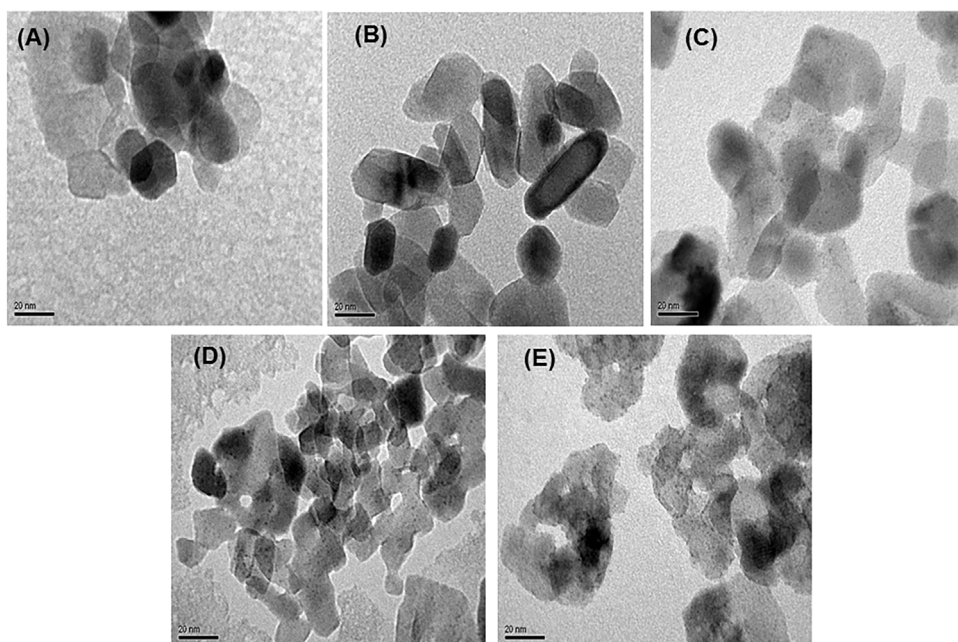


Fig. 4. TEM images of (a) 100Mo, (b) 100V, (c) 100Re, (d) 30Re70Mo, and (e) 30Re70V catalysts. Reduction conditions: 60 mL min⁻¹ H₂, heating rate 10 °C min⁻¹, 500 °C, 3 h. Passivation conditions: 30 mL min⁻¹ 5% O₂/N₂, 2.5 h.

– reveal highly dispersed Re particles of uniform size (about 1 nm). It was not possible to distinguish between the metallic and oxidic components of Re; however, it is highly likely that the particles observed are Re metal since clear distinction between the other oxidic components (Mo or V) and the support was not observed.

FTIR spectra of the support and the catalysts (Fig. 5) show bands with a maximum within the 3370–3410 cm⁻¹ region and at 1630 cm⁻¹ assigned to ν(OH) stretching and bending modes, respectively, of adsorbed water. The unresolved band around 3200 cm⁻¹ is attributed to hydroxyl groups associated with highly dispersed MoO_x and VO_x species since no bands corresponding to crystalline Mo and V oxides were detected, which agrees with XRD results. The literature provides a pictorial representation of the structure of the highly dispersed molybdenum and vanadium oxide on TiO₂ support: the molecular structure of MoO₃/TiO₂ is postulated to be a O–MoO₄ monomer with a single O–Mo double bond, and with four bridging oxygen links to the surface [55]; on the other hand, the molecular structure of V₂O₅/TiO₂ consists of monomeric O–VO₃ species with a single O–V double bond, and with three bridging V–O-support bonds [56]. Therefore, the expected stronger interaction of these oxides with TiO₂ should have implications in the generation of coordinatively unsaturated

sites [55,57]. Upon Re introduction, new bands with maximum at 1400 cm⁻¹ and 920 cm⁻¹ assigned to bending vibration of Re–OH and terminal Re–O bond stretching mode, respectively, are observed, supporting our hypothesis [58,59].

H₂-TPR analysis was used to ascertain the nature of the species present on the screened catalysts. H₂-TPR profiles – together with their Gaussian deconvolution peaks – of calcined Re-based catalysts are comparatively shown in Fig. 6. The profile for the bare TiO₂ support, shown in Fig. 6a, presents a broad reduction peak with a maximum at 508 °C which originates from the surface reduction of TiO₂ (the H₂ consumption value corresponds to stoichiometric reduction of Ti⁴⁺ to Ti^{+3.94}). The H₂ consumption peaks of the 100Mo catalyst (Fig. 6a) was fitted to four main peaks with maxima at 387, 439, 630 and 727 °C: the two low-temperature peaks are attributed to the reduction of octahedrally coordinated Mo, while the latter two peaks are assigned to the reduction of tetrahedrally coordinated Mo [60] and peaks associated with the support masked by the MoO₃ reduction peaks. Hydrogen consumption values indicate that the 100Mo catalyst was stoichiometrically reduced to the oxidation state of +4.4 at 500 °C. TPR profiles of Re–MoO_x/TiO₂ catalysts show that the addition of Re to MoO_x/TiO₂ has a substantial effect on the reduction behavior: the intensity of the wide and convoluted peaks

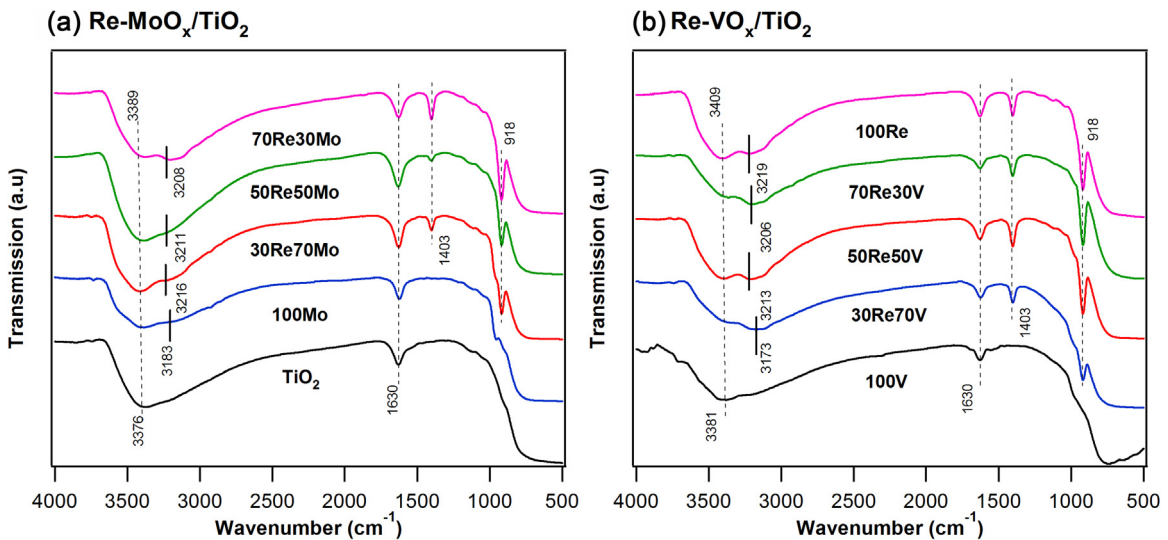


Fig. 5. FTIR spectra of calcined (a) Re-MoO_x/TiO₂ and (b) Re-VO_x/TiO₂ catalysts.

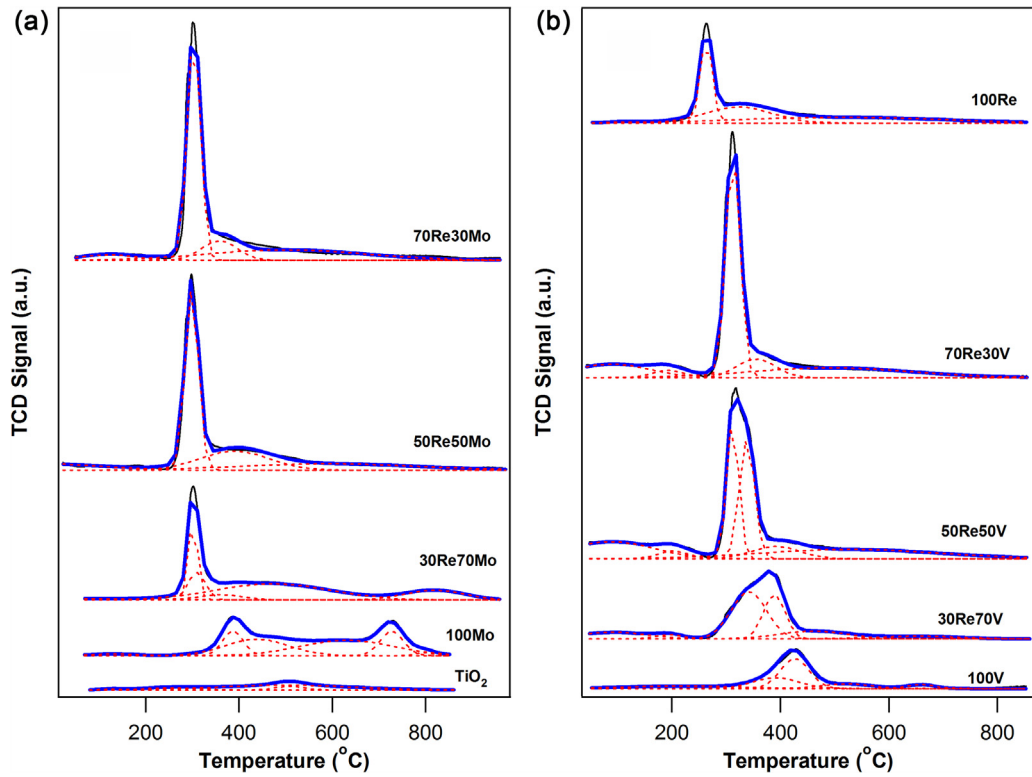


Fig. 6. H₂-TPR of calcined (a) Re-MoO_x/TiO₂ and (b) Re-VO_x/TiO₂ catalysts. Reduction conditions: 50 mL min⁻¹ 5% H₂/Ar, heating rate 10 °C min⁻¹.

that characterize the reduction of the 100Mo catalyst decreases considerably, while the lower-temperature peak which signals the reduction of the 100Re catalyst shifts from 40 °C to 300 °C, an evidence of close contact between Re and MoO_x species. An increase in Re content (or a decrease in Mo content) causes an increase of the intensity of the main peak and a concomitant decrease of the intensity of the higher-temperature peaks without affecting the reduction temperature, demonstrating that the nature of the surface species remains unchanged with metal content.

The H₂-TPR profiles of the Re-VO_x/TiO₂ catalysts are shown in Fig. 6b. For the 100V catalyst, one prominent reduction peak at 426 °C can be observed, in good agreement with vanadia-titania catalysts [61,62]; however, deconvolution reveals two overlapping

peaks with maxima at 391 and 426 °C. The amount of H₂ consumed implies that these peaks accounts for the sequential reduction of V₂O₅ to V₂O₃ (V⁵⁺ → V⁴⁺ → V³⁺) [62]. In addition, the shoulder with a maximum at 523 °C is associated to the support while the small peak at 659 °C corresponds to the reduction of strongly interacting V₂O₅ crystallites. The Re-VO_x/TiO₂ catalysts present one prominent broad peak, which has been resolved into two contributing peaks, positioned between the relative reduction temperatures of monometallic 100Re and 100V ones. This is consistent with strong interaction between Re and VO_x species, similar to the Re-MoO_x/TiO₂ catalysts. Table 2 shows that H₂ consumption increases with increasing Re content for both series.

Table 2H₂-TPR and NH₃-TPD results of Re-MoO_x/TiO₂ and Re-VO_x/TiO₂ catalysts.

Samples	H ₂ consumption		Acidity (mmol NH ₃ g _{cat} ⁻¹)			Acid site density (μmol m ⁻²)	
	mmol g _{cat} ⁻¹	mol H ₂ · mol _M ^{-1a}	Weak T < 300 °C	Medium 300 °C < T < 500 °C	Strong T > 500 °C	Total	
TiO ₂	0.6	–	0.30	0.22	0.04	0.56	3.6
100Mo	2.5	2.8	0.25	0.09	0.03	0.37	2.8
30Re70Mo	2.7	2.2	0.20	0.16	0.05	0.41	3.6
50Re50Mo	3.4	3.1	0.24	0.07	0.01	0.32	3.2
70Re30Mo	3.8	3.7	0.17	0.07	0.01	0.25	3.7
100Re	1.7	5.8	0.28	0.11	0.06	0.45	3.1
100V	1.1	1.3	0.13	0.04	0.00	0.17	2.3
30Re70V	2.1	1.7	0.16	0.05	0.03	0.24	3.5
50Re50V	3.6	3.4	0.16	0.09	0.03	0.28	4.4
70Re30V	3.7	4.0	0.11	0.04	0.01	0.16	3.3

^a mol H₂ · mol_M⁻¹ is amount of H₂ consumed per mole of total metal content.**Table 3**XPS binding energies and surface atomic ratios for Re-MoO_x/TiO₂ and Re-VO_x/TiO₂ catalysts.

Entry	Catalyst	Binding energy (eV) (distribution [%])					Surface atomic ratio (at/at)			
		Ti 2p _{3/2}	O 1s	Re 4f _{7/2}	Mo 3d _{5/2}	V 2p _{3/2}	Re/Ti	Mo(V)/Ti	(Re+Mo[V])/Ti	Re/Mo
1	TiO ₂	458.6	530.0	–	–	–	–	–	–	–
2	100Re	458.6	529.9	40.0 (60) 42.1 (40)	–	–	0.194	–	–	–
3	100Mo	458.6	529.9	–	229.5 (32) 231.5 (68)	–	–	0.202	–	–
4	30Re70Mo	458.6	530.01	40.1 (72) 41.0 (28)	229.1 (60) 231.7 (40)	–	0.522	0.206	0.728	2.53
5	50Re50Mo	458.6	529.9	40.0 (65) 42.1 (35)	229.2 (51) 231.5 (49)	–	0.298	0.116	0.414	2.57
6	70Re30Mo	458.6	530.0	40.0 (51) 41.3 (49)	229.3 (51) 231.8 (49)	–	0.228	0.092	0.320	2.48
7	100V	458.6	529.9	–	–	516.0	–	0.125	–	–
8	30Re70V	458.6	530.0	39.8 (70) 42.0 (30)	–	514.5 (28) 516.0 (72)	0.574	0.165	0.739	3.48
9	50Re50V	458.6	529.9	40.6 (69) 42.3 (31)	–	514.3 (27) 515.8 (73)	0.316	0.101	0.417	3.13
10	70Re30V	458.6	530.0	40.8 (58) 42.7 (42)	–	513.9 (41) 515.2 (59)	0.241	0.046	0.287	5.24

The surface chemical composition of the reduced-passivated catalysts was characterized by XPS and listed in **Table 3**. The binding energy (BE) of Ti 2p_{3/2} core-level in the support and the catalysts is 458.6 eV, which is assigned to Ti⁴⁺ (TiO₂) [63]. This indicates that TiO₂ was not reduced at the reduction temperature of 500 °C, in agreement with TPR results which indicates only partial reduction of the surface. **Fig. 7a** shows the Mo 3d core-level spectra of the Re-MoO_x/TiO₂ catalysts (also summarized in **Table 3**). The spectra display the characteristic Mo 3d doublet, whose spin-orbit splitting (3d_{5/2} and 3d_{3/2}) is 3.2 eV. Peak deconvolution reveals two partially overlapped Mo 3d doublets with BE of 229.3 ± 0.2 eV characteristic of Mo⁴⁺ and 231.6 ± 0.2 eV assigned to Mo⁵⁺ [64,65]. These values are consistent with the formation of partially-reduced MoO_x moieties during H₂ reduction, and generation of coordinatively unsaturated sites (CUS) of MoO₂ [25,66]. The distribution of oxidation states, given in parenthesis in **Table 3**, shows that Mo⁵⁺ predominates in the 100Mo catalyst; however, the surface concentration of Mo⁴⁺ increases upon addition of Re species, agreeing with TPR results that Re promoted the reduction of Mo oxide. The Re 4f core-level spectra of the 100Re and the Re-MoO_x/TiO₂ catalysts (**Fig. 7b**) show the characteristic Re 4f doublet whose spin-orbit splitting (4f_{7/2} and 4f_{5/2}) is 2.4 eV. The Re 4f_{7/2} signal with BE at 40.0 eV corresponds to Re⁰ [67,68], while the BEs observed in the range 41.0–42.1 eV are associated with oxidized ReO_x species [Re⁴⁺ and Re^{δ+} (0 < δ < 4)], indicating incomplete reduction of Re oxide [28]. The broad BE interval observed for ReO_x species attests to different degrees of partial reduction due to different loadings of Re

and Mo. **Table 3** shows that the surface concentration of Re⁰ and ReO_x species was slightly influenced by the presence of MoO_x.

XPS results of Re-VO_x/TiO₂ catalysts are shown in **Fig. 8**: (a) V 2p core-level spectra and (b) the corresponding Re 4f core-level spectra. The V 2p core-level spectra show the characteristic V 2p doublet whose spin-orbit splitting (2p_{3/2} and 2p_{1/2}) is 7.5 eV. The V 2p_{3/2} signals observed between 515.2 and 516.0 eV correspond to V⁴⁺ species, while the signals observed between 513.9 and 514.5 eV are associated with V²⁺³⁺ species [69]. The presence of these species indicates partial reduction of V oxide during H₂ reduction and also creation of CUS sites [25,57], similar to the Mo-oxide counterparts. Notably, surface vanadium oxide is reduced only to V⁴⁺ on the 100V catalyst, while upon Re incorporation it is reduced to both V⁴⁺ and V²⁺³⁺. This is in line with TPR results, confirming that the interaction between Re and VO_x promotes the reduction of VO_x. The Re 4f_{7/2} signal (**Fig. 8b**) between 39.8 and 40.8 eV is associated with Re⁰, and between 42.0 and 42.7 eV is close to binding energies reported for Re⁴⁺ species of ReO₂ [67].

The concentration of surface dispersed Re, Mo and V species on the support can be estimated from surface Re/Ti, Mo/Ti and V/Ti atomic ratios, listed in **Table 3**. The results show that at the same Re/MoO_x (or VO_x) loading, the surface coverage of MoO_x species was higher than VO_x species in their respective catalysts. This is consistent with specific surface area results which indicated preferential deposition of vanadium oxide nanoparticles inside the support pores. **Table 3** also shows that the presence of MoO_x or VO_x species significantly enhances the surface enrichment of Re species, indicating that the interactions between Re and MoO_x (or VO_x) are

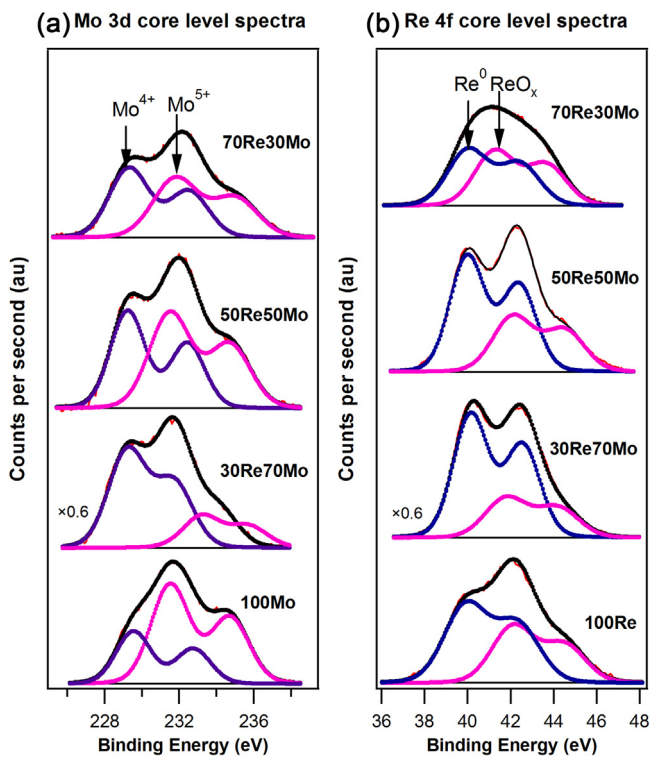


Fig. 7. (a) Mo 3d and (b) Re 4f core-level spectra of the reduced-passivated Re-MoO_x/TiO₂ catalysts. Reduction conditions to remove the oxidation layer: 50 mL min⁻¹ H₂, 300 °C, 1 h.

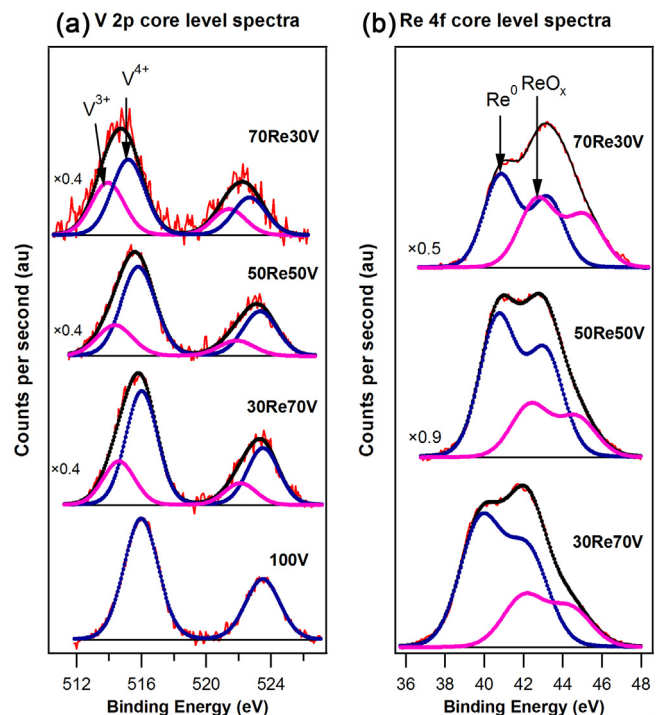


Fig. 8. (a) V 2p and (b) Re 4f core-level spectra of the reduced-passivated Re-VO_x/TiO₂ catalysts. Reduction conditions to remove the oxidation layer: 50 mL min⁻¹ H₂, 300 °C, 1 h.

stronger than the interaction between Re and TiO₂ support [70]. The effect of Re and Mo (or V) loading on the surface coverage of the metal/metal oxide species provides insights into the partial migration of the species towards the surface of the catalysts. As expected,

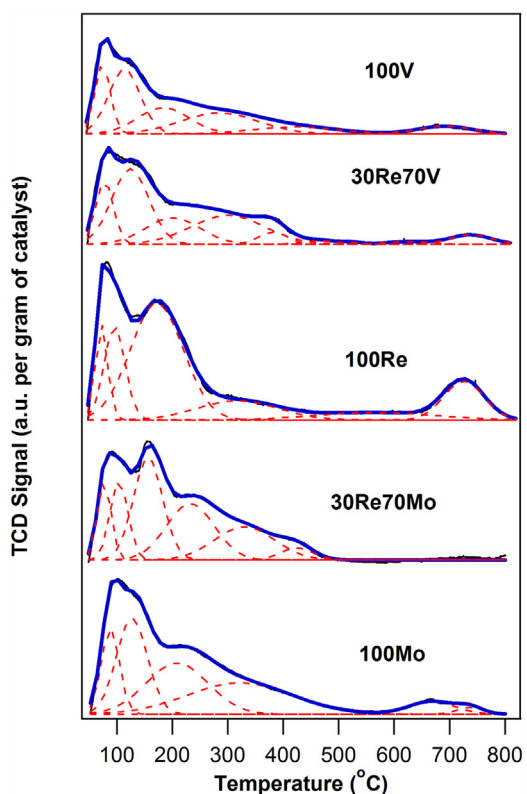


Fig. 9. H₂-TPD of a selection of reduced catalysts. Reduction conditions: 50 mL min⁻¹ 5% H₂/Ar, heating rate 10 °C min⁻¹. H₂-TPD conditions: 50 mL min⁻¹ He, heating rate of 10 °C min⁻¹.

the surface Mo/Ti and V/Ti atomic ratios decrease with decreasing Mo and V loading, respectively. In contrast, Re surface coverage decreases with an increase of Re loading in both catalyst series. These results suggest that an increase in Re content (decrease in Mo or V) increased the redistribution and migration of MoO_x and VO_x species to decorate the surface Re species due to close contact between Re and Mo (or V), in accordance with previous reports in other metal/metal oxide systems [29,37,71,72]. Moreover, the surface coverage of Re and Mo (or V) species for these two series is noticeably similar.

H₂-TPD profiles were obtained for selected catalysts, 100Re, 100Mo, 100V, 30Re70Mo and 30Re70V. As will be discussed later, differences in products selectivity were observed, primarily, between 100Re and 100Mo (or 100V), and upon addition of Re to MoO_x/TiO₂ or VO_x/TiO₂. Aside from the nature of catalytic sites, the observed differences could also be due to the hydrogen adsorption capability of the catalysts; therefore, the H₂ desorption profiles of the aforementioned catalysts are presented in Fig. 9. The TPD profiles were deconvoluted into multiple peaks which correspond to different nature of adsorbed hydrogen. All the catalysts show an intense low-temperature peak (<90 °C) which may be associated with molecularly adsorbed hydrogen on the support. Multiple overlapping peaks appearing within 90–600 °C range are either associated with molecularly adsorbed hydrogen (90–300 °C) or dissociatively adsorbed hydrogen (300–600 °C) on the metal/metal oxide species [73]. The origin of the dissociated hydrogen atoms is probably different for metals and reducible metal oxides: Based on other literature studies, it is inferred that the hydrogen atoms were derived from those bound to metallic sites (such as Re⁰ on 100Re) or atomic hydrogen inserted into ReO_x, MoO_x and VO_x bronze during reduction of 100Re, 100Mo and 100V, respectively [52,73–75]. For HDO reactions, hydrogenation steps require donation of dissociated hydrogen atoms to adsorbed reactant molecules. Although

it is difficult to precisely determine the ease of donation of dissociated hydrogen atoms, we predict that bound hydrogen atoms on metallic Re sites are more easily delivered than dissolved hydrogen atoms in MoO_x or VO_x bronze. This assertion is also reflected in the distinct desorption at 725 °C by the 100Re catalyst which is assigned to spillover of hydrogen atoms on TiO_2 support, similar to that observed for Pt catalysts [76].

Interestingly, although TPR and XPS results show that the reducibility of Mo and V species was facilitated in the presence of rhenium, H_2 -TPD profiles show no obvious difference between 100Mo and 30Re70Mo or between 100V and 3070V. It appears that any observed changes are associated with modification of the ability of Re species to absorb hydrogen. For example, Fig. 9 shows that spillover hydrogen species which exist on the 100Re catalyst are not observed for 30Re70Mo and significantly decreased for 30Re70V catalysts, suggesting that the interaction between Re and TiO_2 is weakened by the presence of MoO_x and VO_x . A corollary of this observation is that hydrogenation capabilities of 30Re70Mo and 30Re70V are expected to be lower than for the 100Re catalyst.

The critical role of surface acidity of solid catalysts in HDO reactions has been well established [1]. Acid sites have been shown to enhance the adsorption of reactants and intermediates, in addition to catalyzing some classes of reactions occurring during HDO such as dehydration, transalkylation, isomerization and cracking, etc. [1,22]. In this study, the total acidity and acid strength distribution were obtained by NH_3 -TPD analysis. The profiles show desorption peaks over the whole temperature range, implying the presence of acid sites of different strength. The acid site distribution was determined by fitting the TPD curves with a Gaussian function for quantitative deconvolution (not shown) and calculating the area corresponding to weak ($T < 300^\circ\text{C}$), medium ($300^\circ\text{C} < T < 500^\circ\text{C}$) and strong ($T > 500^\circ\text{C}$) acidity [77]. The results of the reduced $\text{Re-MoO}_x/\text{TiO}_2$ and $\text{Re-VO}_x/\text{TiO}_2$ catalyst series are shown in Fig. 10 and summarized in Table 2. Fig. 10 shows that the most intense desorption peak had a maximum in the low temperature region, indicating the predominance of weak acid sites on all the catalysts. The desorption profile of TiO_2 support (Fig. 9a) gives rise to two overlapping peaks in the weak acid temperature range, a well-resolved peak with a maximum at 370 °C and a small shoulder at 500 °C, and a small peak at ca. 630 °C. Although the nature of the acid sites were not determined in this study, the acidity of reducible TiO_2 anatase is well-documented to be associated with unsaturated Ti^{4+} ions and surface hydroxyls [66,78]. The existence of these species on TiO_2 were confirmed by XPS and FTIR results. In Table 2, the total desorbed NH_3 of 0.56 mmol g⁻¹, corresponding to 2.2 molecules per nm², is identical to the reported acid site concentration of TiO_2 anatase [79]. Introduction of MoO_x and VO_x species decreased the acidity, particularly the medium acid sites, attributed to interaction of lower acidic metal oxide species with surface hydroxyl sites. Chary et al. [61,66] reported that Mo and V atoms selectively interact with acidic Ti-OH groups on the TiO_2 surface, while the basic groups on the support are almost not perturbed. The decrease in acidity was more drastic upon VO_x introduction which is consistent with the more pronounced decrease in BET surface area and lower XPS V/Ti ratio of 100V (in comparison to BET surface area and XPS Mo/Ti ratio of 100Mo). Thus, the results indicate that VO_x species preferentially located inside the pores of the support (which are inaccessible by XPS) blocked weak acid sites associated with TiO_2 , and consequently decreased the total acidity. The catalysts displayed similar desorption profiles (Fig. 10a and b): weak acid peaks in the vicinity of the support's indicate the presence of accessible acid sites of the support. However, the low temperature peak at ca. 70 °C of the catalysts was more intense than the support's, indicating contributions from Re, Mo and V sites. Fig. 10 also shows an across-the-board decline in intensity of peaks corresponding to medium acid sites stemming from anchoring of Re and Mo (or V)

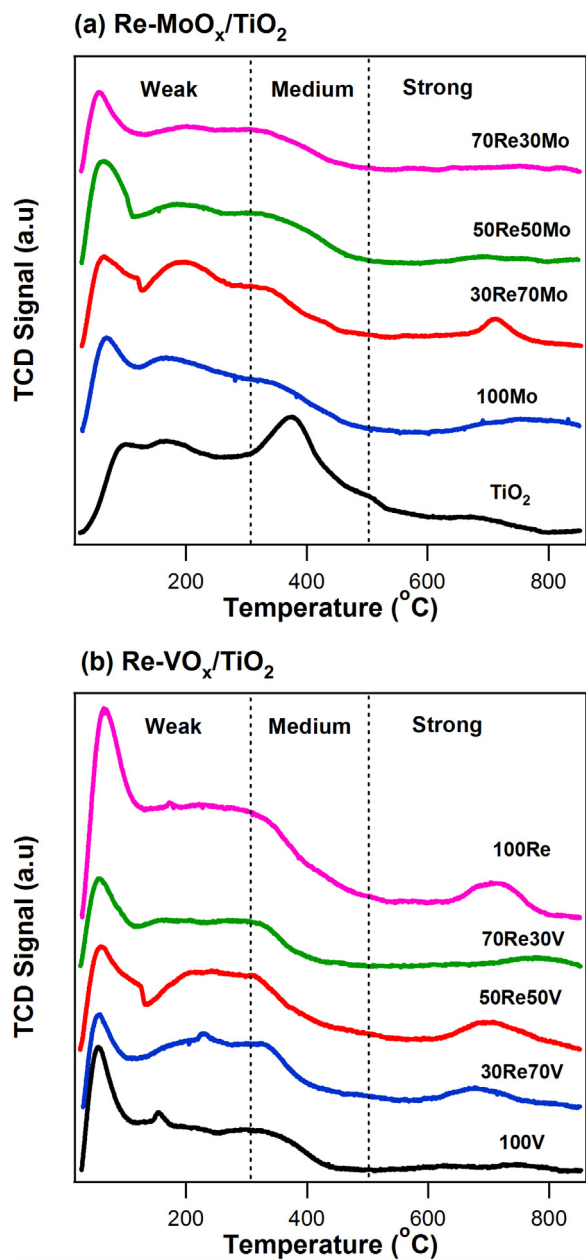


Fig. 10. NH_3 -TPD of reduced (a) $\text{Re-MoO}_x/\text{TiO}_2$ and (b) $\text{Re-VO}_x/\text{TiO}_2$ catalysts. Reduction conditions: $50 \text{ mL min}^{-1} \text{ H}_2$, heating rate $10 \text{ }^\circ\text{C min}^{-1}$, 500°C , 3 h. Passivation conditions: $30 \text{ mL min}^{-1} 5\% \text{ O}_2/\text{N}_2$, 2.5 h.

species on OH sites of the support. Alternatively, reduced Re and Mo or V cations may replace Ti^{4+} sites which could lead to drop in acidity. Distribution of acid sites listed in Table 3 shows the predominance of weak and medium acid sites on the support and also on the catalysts. The strong acid site concentration does not change upon introduction of metal/metal oxide species. For the $\text{Re-MoO}_x/\text{TiO}_2$ and $\text{Re-VO}_x/\text{TiO}_2$ series, the total acidity correlates to the surface $(\text{Re}+\text{Mo}[V])/\text{Ti}$ atomic ratio in Table 3, confirming the contribution of exposed, partially-reduced metal oxide species to the acidity of the catalysts. Notably, despite the similarities in the surface coverage of the metal/metal oxide species, the total acidity of the $\text{Re-VO}_x/\text{TiO}_2$ catalyst was lower than the $\text{Re-MoO}_x/\text{TiO}_2$ counterpart with the same metal loading, indicating that another phenomenon may be in play. It has been reported that differences in metal-oxygen bond energy can be linked to the ability to generate oxygen vacancy sites which function as Lewis acid sites [26].

Table 4

Catalytic results of anisole conversion in a batch reactor at 300 °C and 3 MPa H₂.

Catalyst	Reaction rate	
	Initial ($\times 10^{-6}$ mol _{anisole} g _{catal} s ⁻¹)	Intrinsic ($\times 10^{-4}$ molec _{anisole} atom _(Re+M) ⁻¹ s ⁻¹)
100Mo	3.0	13.1
30Re70Mo	4.1	5.2
50Re50Mo	3.7	8.3
70Re30Mo	2.7	8.0
100Re	2.3	9.9
100V	1.1	7.6
30Re70V	2.3	5.0
50Re50V	2.4	5.2
70Re30V	2.3	7.6

In that regard, Mortensen et al. [26] concluded that introducing metal oxide species to another metal oxide can facilitate creation of more vacancy sites, particularly when there is a large difference in metal-oxygen bond energy. The reported metal-oxygen bond energy (V₂O₃ = 12.3 eV, MoO₂ = 16.7 eV, and ReO₂ = 6.5 eV [80,81]), supports this hypothesis and indicates that adding ReO₂ to MoO₂ generates more Lewis acid sites in comparison to the addition of ReO₂ to V₂O₃.

3.3. Hydrodeoxygenation of Re-MO_x/TiO₂ catalysts

The time-course of the conversion of anisole are shown in Figs. 11 and 12. The concentration of anisole and the products were determined relative to the hexadecane standard. Fig. 11a and b show that the 100Mo and 100V catalysts displayed similar concentration profiles: phenol was the dominant product, while cresols were obtained in significantly lower quantity [3]. Products detected in trace amounts, even at 4 h reaction time, include benzene, methanol, toluene and cyclohexane. These products distribution indicates a low deoxygenation and hydrogenation activity of the 100Mo and 100V catalysts. Fig. 11c shows that anisole conversion over the 100Re catalyst is mainly phenol, benzene, cresols and cyclohexane, and toluene as trace. The difference in the concentration profiles between the 100Re and 100Mo (or 100V) catalysts indicates differences in the nature of the active sites catalyzing the conversion of anisole.

The time-course of the conversion of anisole over TiO₂-supported Re-MO_x and Re-VO_x catalysts are depicted in Fig. 12a and b, respectively. For the former, benzene was the major product over the 30Re70Mo and 50Re50Mo catalysts, and phenol, cresols and toluene were present in appreciable amounts. Barely any saturated hydrocarbons were detected over these catalysts. Over the 70Re30Mo catalyst, anisole was converted to mostly phenol and benzene, while saturated hydrocarbons and cresols were obtained in lower quantities (toluene was detected in traces). Fig. 12b shows that the concentration profiles of the products from the conversion of anisole over Re-VO_x/TiO₂ catalysts were similar to the Re-MO_x/TiO₂ catalysts. Judging by the concentration profiles, phenol was an intermediate product over both catalytic series.

The initial reaction rate of the catalysts is given in Table 4. The Weisz-Prater and Mears criteria were used to confirm the absence of internal and external mass transfer limitations for the highest rate observed (Supplementary information). The monometallic catalysts decreased in the order: 100Mo > 100Re > 100V, while the addition of Re to MoO_x/TiO₂ and VO_x/TiO₂ increased the initial reaction rates relative to 100Mo and 100V, respectively. The observed differences in activity can neither be explained by differences in particle size obtained from XRD and TEM data, nor by surface acidity derived from NH₃-TPD result. As previously discussed, XRD and TEM results did not show clear crystallite size difference between the catalysts; while NH₃-TPD data show that the catalysts contain

similarly low concentration of strong acid sites. Thus, the difference in reactivity appears to be linked to reactivity of surface species or nature of the catalytic sites. For the binary catalysts, the activity of the Re-VO_x/TiO₂ catalysts were identical while that of the Re-MoO_x/TiO₂ catalysts decreased with increasing Re content (i.e. 30Re70Mo > 50Re50Mo > 70Re30Mo).

To elucidate the relative reactivity of the surface species, the catalytic activity is expressed as the intrinsic reaction rate which is the initial reaction rate normalized by exposed surface species (derived from XPS surface atomic ratio), calculated according to the equation:

$$\text{Intrinsic rate}(\text{molec}_{\text{anisole converted}}/\text{atom}_{(\text{Re}+\text{M})} \cdot \text{s})$$

$$= \frac{r_S \times \text{MW}_{\text{TiO}_2}}{[1 - (Wt_{\text{Re}} + Wt_M)] \cdot \text{gm} \times [(Re + M)/Ti]_{\text{XPS}}}$$

where M is either Mo or V, r_S is the initial reaction rate ($\text{mol g}^{-1} \text{s}^{-1}$), MW_{TiO_2} is the molar mass of TiO₂ (79.86 g mol⁻¹); Wt_{Re} is the Re loading (wt.%), Wt_M is the Mo or V loading, and $(Re+M/Ti)_{\text{XPS}}$ is the total XPS surface atomic Re+M/Ti ratio (atom atom⁻¹). The intrinsic rate is listed in Table 4 and illustrated in Fig. 13. Discrepancies on the nature of the catalytic sites on partially reduced MoO₃ and ReO₃ catalysts for the HDO of phenolic compounds have been continuously reported. Recent studies, however, provides insight into the surface sites: Prasomsri et al. [3] reported MoO_xC_yH_z or MoO_{3-x} phases containing Mo⁵⁺ as active sites and Mo⁴⁺ to be non-active in the HDO of anisole. On the other hand, Leiva et al. [28] credited the higher activity of ReO_x/SiO₂ over Re/SiO₂ to the presence of ReO_x phase containing Re^{δ+} ($0 < \delta < 4$) and Re⁴⁺ species. Our results agree with these observations. Fig. 13 shows the 100Mo catalyst to be more active than the 100Re one, suggesting that Mo⁵⁺ species are intrinsically more active than Re⁴⁺ species. In fact, this is reflected in the observed intrinsic activity trend of the Re-MoO_x/TiO₂ catalysts (see the relative abundance of Mo oxidation states for entries 3–6 in Table 3): the drop in activity upon Re loading (for the 30Re70Mo catalyst) coincides with the over-reduction to Mo⁴⁺ (i.e. entry 3 and 4 shows that the fraction of Mo⁵⁺ decreases from 68% to 40%); the activity then increased upon further increase of Re content (and decrease of Mo content) due to the modest increase in Mo⁵⁺ sites (entries 5 and 6); and finally, the identical activity of the 50Re50Mo catalyst is in line with the two catalysts having the same fraction of Mo⁵⁺ sites. The correlation of the intrinsic reaction rate with the fraction of Mo⁵⁺ cation agrees with the results of Prasomsri et al. [3], and also indicates that Mo⁵⁺ sites have more control over Re sites on the activity of Re-MoO_x/TiO₂ catalysts.

In contrast, the activity, for Re-VO_x/TiO₂, appears to be controlled by the surface fraction of Re⁴⁺ due to the fact that the 100Re catalyst exhibited a higher intrinsic reaction rate than the 100V one (Fig. 13). Addition of Re to VO_x decreases the fraction of surface Re⁴⁺ sites (the 30Re70V and 50Re50V catalysts), leading to a decline in activity. In the case of the 70Re30V catalyst, the fraction of surface Re⁴⁺ species is restored to the level of the 100Re one but the activity still lagged behind the monometallic catalyst, indicating that vanadium site contributions cannot be neglected. The nature of the active sites on vanadium oxide catalysts for HDO reactions has still not been elucidated. Even though Liu et al. [82] revealed a close relationship between TOF and the fraction of V³⁺ ion on VO_x/Al₂O₃ catalyst for propane dehydrogenation, our data does not allow us to determine which of the lower valence state (V⁴⁺ or V³⁺) is the more active site. It is clear, however, that their presence suppressed the activity of ReO_x sites.

In Fig. 14 the products selectivity calculated at 10% conversion shows a similar behavior for the 100Mo and 100V catalysts: high selectivity to phenol (>76%), indicating that demethylation

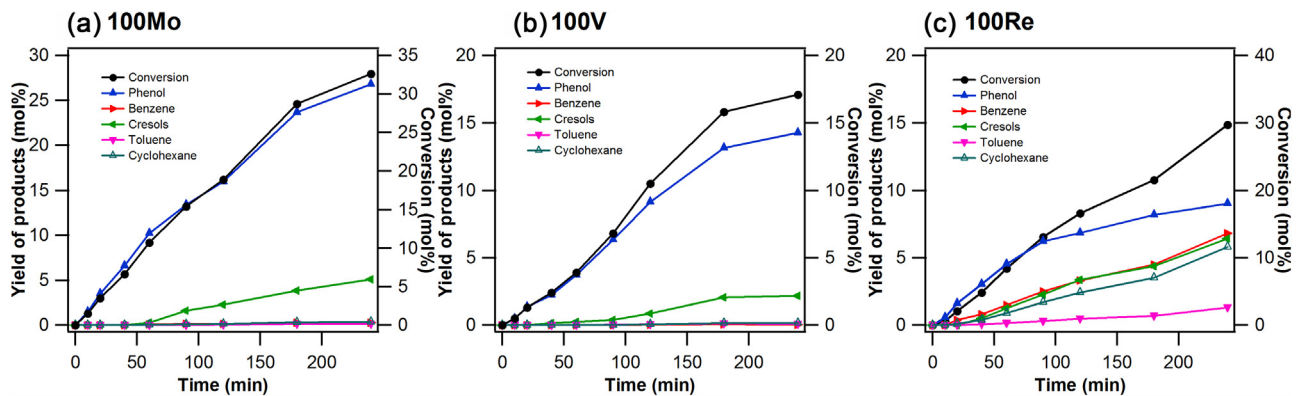


Fig. 11. Conversion and yield of products as a function of time during the conversion of anisole over (a) 100Mo, (b) 100V and (c) 100Re catalysts. Reaction conditions: anisole (19.04 mmol), catalyst (200 mg), dodecane (80 mL), 300 °C, 3 MPa H₂, 4 h.

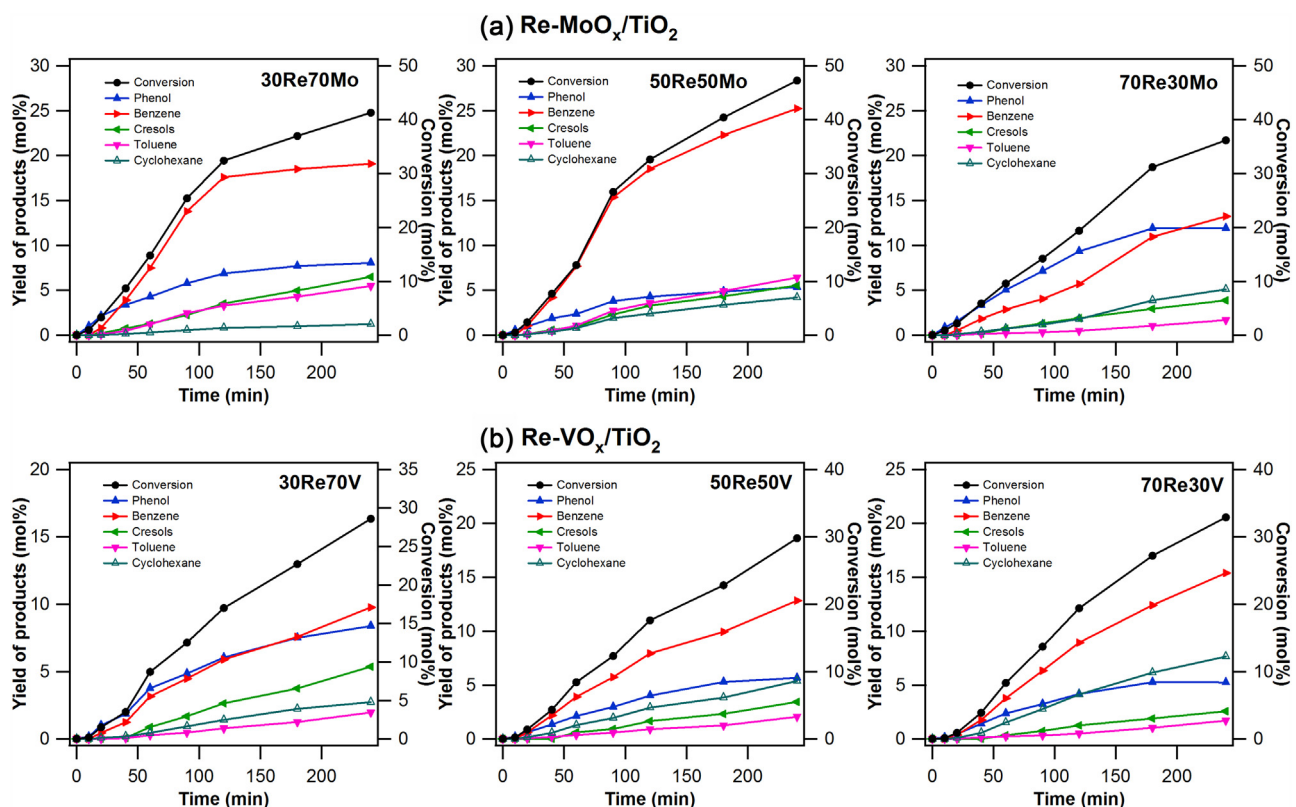


Fig. 12. Conversion and yield of products as a function of time during the conversion of anisole over (a) Re-MoO_x/TiO₂ and (b) Re-VO_x/TiO₂ catalysts. Reaction conditions: anisole (19.04 mmol), catalyst (200 mg), dodecane (80 mL), 300 °C, 3 MPa H₂, 4 h.

of anisole is the primary route. It has been reported that after adsorption of anisole on vacancy sites (on reducible TiO₂ and/or MO_x species), DME proceeds on both metallic and acid sites albeit through different mechanisms [83]. The presence of acidic sites on the catalysts have been demonstrated by XPS and NH₃-TPD results, which further explains the large amount of phenol produced. On the other hand, there was no evidence of direct deoxygenation (DDO) of anisole to benzene over these catalysts, attributed to the absence of metallic sites to aid in the dissociation of H₂. As previously described, after adsorption of anisole on oxygen vacancies of partially reduced surface metal oxides, activated hydrogen can facilitates C–O bond cleavage by protonating the oxygen [42] or by partially hydrogenating the phenolic ring to temporarily remove the delocalization effect of out of plane lone pair orbital [22]. This is especially evident by the 17% benzene selectivity over the 100Re

catalyst. The co-presence of hydrogen activation sites (reduced Re⁰) and coordinatively unsaturated metal sites (ReO_x) confers bifunctional catalytic behavior on the 100Re one. In addition, the production of cyclohexane over the 100Re catalyst, and the absence of it over the 100Mo and 100V catalysts, further evidences the ease of donation of bound hydrogen atoms on metallic Re sites than dissolved hydrogen in MoO_x and VO_x bronze, as inferred from H₂-TPD analysis. Fig. 14 also shows that the 100Re catalyst was more selective towards cresols than the 100Mo and 100V ones, indicating a higher hydroalkylation activity of 100Re. Finally, cresols, formed from the substitution of methyl carbonium ion into the aromatic nucleus, reportedly occur on acid sites [22,83]. Hence, the small amounts of cresols observed over all the catalysts is in line with the low concentration of strong acid sites, as illustrated in Table 2.

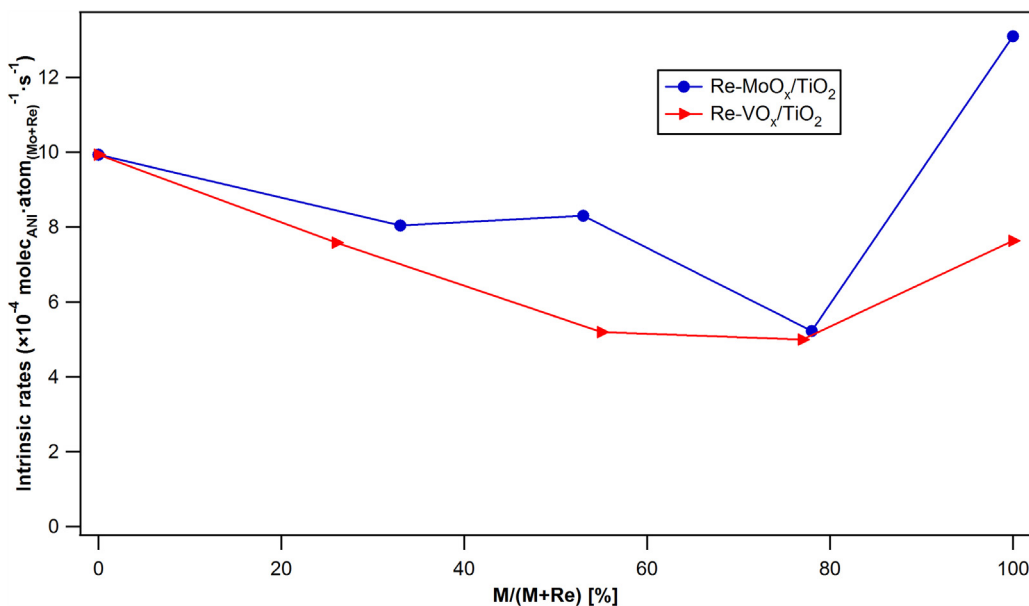


Fig. 13. Intrinsic rates of anisole conversion vs. Mo/(Mo+Re) or V/(V+Re). Reaction conditions: anisole (19.04 mmol), catalyst (200 mg), dodecane (80 mL), 300 °C, 3 MPa H₂, 4 h.

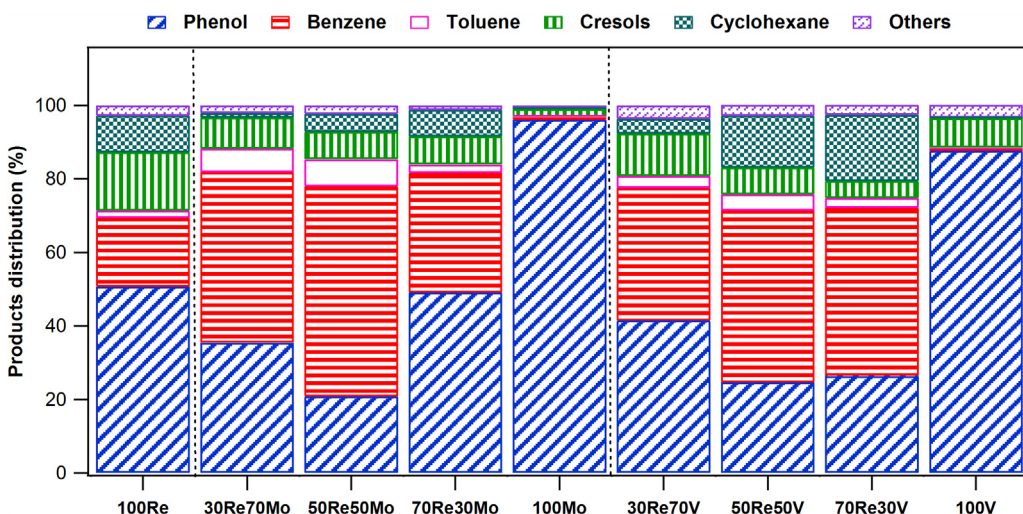


Fig. 14. Product selectivity calculated at 10% anisole conversion over Re-Mo_x/TiO₂ and Re-VO_x/TiO₂ catalysts. Reaction conditions: anisole (19.04 mmol), catalyst (200 mg), dodecane (80 mL), 300 °C, 3 MPa H₂, 4 h.

Other than that, acidity did not play an important role in the product selectivity of the Re-containing catalysts due to the identical concentration of strong acid sites on the catalysts. The selectivity to benzene is more than doubled when Re species are paired with MoO_x and VO_x sites (30Re70Mo and 30Re70V catalysts). Previous report by Prasomsri et al. [27], that coordinatively unsaturated sites of surface Mo and V cations enhance the adsorption of anisole and accordingly bolster the preference for direct deoxygenation, supports this result. It is important not to discount the influence of electronic modification of the catalytic sites on the two-fold increase in benzene selectivity because TPR results provide evidence of close contact between Re and Mo (or V) which could induce electronic modification of Mo and V sites. It is widely known that electronic interaction between a metal additive (Re) and a low oxidation state metal oxide (Mo or V) can arise from the formation of dispersed particles of bimetallic clusters on the support, or the formation of metal clusters that react with the low oxidation state metal cation bound to the support surface (metal–metal bond) [84].

Noticeably, the Re-Mo_x/TiO₂ and Re-VO_x/TiO₂ catalysts with the equimolar metal ratio were the most selective to aromatic hydrocarbons (benzene and toluene) among their respective series. The reason is not yet clear but could be due to electronic effect stemming from close interaction between Re and Mo (or V) species in appropriate proportions in the catalysts. This assertion is further confirmed by the sharp decrease in benzene selectivity on the 70Re30Mo catalyst with respect to the 50Re50Mo one: the disproportionate combination of Re and Mo species led to an increase in the metallic character of the catalyst and, as a consequence, an enhancement in its propensity for breaking O–CH₃ bond at the expense of DMO and/or DDO. Interestingly, this behavior does not extend to the 70Re30V catalyst which presents the same benzene selectivity as the 50Re50V one, which points out a less drastic effect on the nature of the active sites of Re-VO_x/TiO₂ with increasing Re content (decreasing V content) above a certain point.

Fig. 15 shows that BTX selectivity of the Re-containing catalysts initially increased with conversion and then plateaued afterwards

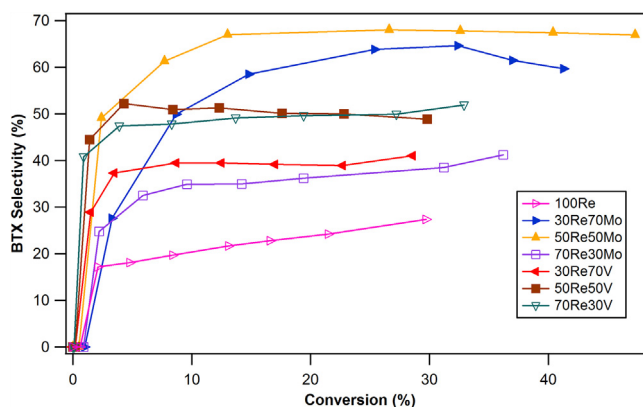


Fig. 15. BTX selectivity as a function of conversion of Re-containing catalysts. Reaction conditions: anisole (19.04 mmol), catalyst (200 mg), dodecane (80 mL), 300 °C, 3 MPa H₂, 4 h.

(except for the 30Re70Mo catalyst which decreased slightly). As shown schematically in Fig. 1, HDO of anisole involves consecutive reactions which include hydrogenation of benzene and toluene to cyclohexane and methylcyclohexane, respectively, and thus it is conceivable that the concentration of BTX will diminish at higher anisole conversion. This was, however, not the case for the Re-MO_x/TiO₂ catalysts within the range of observed conversion. To determine ring hydrogenation capability, the 50Re50Mo catalyst was tested for hydrogenation of benzene and toluene following the same procedure and reaction conditions used for the conversion of anisole: only a minor fraction of benzene and toluene was converted (3%) after 4 h, which is consistent with the low amount of cyclohexane and methylcyclohexane observed from anisole conversion. In contrast, other studies reportedly observed copious amount of these products primarily because cyclohexanol and methylcyclohexanol, which can be more readily converted to cyclohexane or methylcyclohexane, respectively, were prominent intermediates in their reactions [9,11]. Therefore, the minimal amounts of hydrocarbons obtained reflect the Re-MO_x/TiO₂ catalysts preference for the direct demethoxylation and/or deoxygenation pathway to produce aromatic hydrocarbons over the hydrogenation route to produce aromatic alcohols. The significant fraction of aromaticity retained within the range of conversion underscores the potential of Re-MO_x/TiO₂ and Re-VO_x/TiO₂ catalysts for selective lignin valorization. To put these results in a broader context, anisole conversion after 4 h over the best catalyst was slightly lower than the results of Jongerius et al. [4] with commercial presulfided CoMo/Al₂O₃ catalyst under comparable reaction conditions, while the BTX selectivity was more than 4 times higher, providing a template to further improve the capabilities and performances of these catalysts.

4. Conclusion

This study reports the conversion of anisole over a series of metal/metal oxide catalysts, producing mostly phenol from demethylation. The inability of the Ni-, Co- and Ga-based catalysts to catalyze the conversion of anisole to benzene renders them unsuitable for HDO of phenolic compounds. On the other hand, due to its oxophilicity, the Re catalyst stood out for its unique ability for the production of aromatic hydrocarbons. Combining Re with lower oxidation states Mo and V cations dramatically increases selectivity to desired benzene and toluene, attributed to enhanced adsorption of anisole on surface oxygen vacancy sites of MO_x or VO_x. However, this increase is contingent on combinations of Re and Mo (or V) in appropriate proportions which is consistent with the existence of synergism between Re and MO_x species. Activity difference was

related to the nature of catalytic sites: the decrease in the fraction of surface Mo⁵⁺ sites is alluded to as the reason for the diminished activity of Re-MO_x/TiO₂ catalyst in comparison to MO_x/TiO₂ one. This observation was not confined only to this series, although Re⁴⁺ species appear to be the dominant sites on the Re-VO_x/TiO₂ catalysts during the conversion of anisole. The study emphasizes the importance of preparing catalysts that exhibit specific sites needed for desired product formation.

Acknowledgements

This work was supported by CONICYT-Chile under FONDECYT projects Nos. 3150033 and 1140528. The authors also gratefully acknowledge the financial support under PFB-27 and FONDEQUIP EQM 120096 grants.

Appendix A. Supplementary data

Supplementary data associated with this article can be found, in the online version, at <http://dx.doi.org/10.1016/j.apcatb.2017.02.047>.

References

- [1] M. Saidi, F. Samimi, D. Karimipourfard, T. Nimmanwudipong, B.C. Gates, M.R. Rahimpour, Energy Environ. Sci. 7 (2014) 103–129.
- [2] J. Zakzeski, P.C.A. Bruijnincx, A.L. Jongerius, B.M. Weckhuysen, Chem. Rev. 110 (2010) 3552–3599.
- [3] T. Prasomsri, M. Shetty, K. Murugappan, Y. Roman-Leshkov, Energy Environ. Sci. 7 (2014) 2660–2669.
- [4] A.L. Jongerius, R. Jastrzebski, P.C.A. Bruijnincx, B.M. Weckhuysen, J. Catal. 285 (2012) 315–323.
- [5] V.N. Bui, D. Laurenti, P. Afanasiev, C. Geantet, Appl. Catal. B 101 (2011) 239–245.
- [6] A. Gutierrez, R.K. Kaila, M.L. Honkela, R. Slioor, A.O.I. Krause, Catal. Today 147 (2009) 239–246.
- [7] A.K. Deepa, P.L. Dhepe, ChemPlusChem 79 (2014) 1573–1583.
- [8] R.C. Runnebaum, T. Nimmanwudipong, D.E. Block, B.C. Gates, Catal. Sci. Technol. 2 (2012) 113–118.
- [9] S.A. Khromova, A.A. Smirnov, O.A. Bulavchenko, A.A. Saraev, V.V. Kaichev, S.I. Reshetnikov, V.A. Yakovlev, Appl. Catal. A 470 (2014) 261–270.
- [10] Y. Yang, C. Ochoa-Hernández, V.A. de la Peña O’Shea, P. Pizarro, J.M. Coronado, D.P. Serrano, Appl. Catal. B 145 (2014) 91–100.
- [11] S. Jin, Z. Xiao, C. Li, X. Chen, L. Wang, J. Xing, W. Li, C. Liang, Catal. Today 234 (2014) 125–132.
- [12] T.M. Sankaranarayanan, A. Berenguer, C. Ochoa-Hernández, I. Moreno, P. Jana, J.M. Coronado, D.P. Serrano, P. Pizarro, Catal. Today 243 (2015) 163–172.
- [13] T. Mochizuki, S.-Y. Chen, M. Toba, Y. Yoshimura, Appl. Catal. B 146 (2014) 237–243.
- [14] S. Ted Oyama, T. Onkawa, A. Takagaki, R. Kikuchi, S. Hosokai, Y. Suzuki, K.K. Bando, Top. Catal. 58 (2015) 201–210.
- [15] H.Y. Zhao, D. Li, P. Bui, S.T. Oyama, Appl. Catal. A 391 (2011) 305–310.
- [16] K. Li, R. Wang, J. Chen, Energy Fuels 25 (2011) 854–863.
- [17] W.-S. Lee, Z. Wang, R.J. Wu, A. Bhan, J. Catal. 319 (2014) 44–53.
- [18] A.L. Jongerius, R.W. Gosselink, J. Dijkstra, J.H. Bitter, P.C.A. Bruijnincx, B.M. Weckhuysen, ChemCatChem 5 (2013) 2964–2972.
- [19] C. Zhao, W. Song, J.A. Lercher, ACS Catal. 2 (2012) 2714–2723.
- [20] C. Zhao, J.A. Lercher, ChemCatChem 4 (2012) 64–68.
- [21] W. Song, Y. Liu, E. Barath, C. Zhao, J.A. Lercher, Green Chem. 17 (2015) 1204–1218.
- [22] X. Zhu, L.L. Lobban, R.G. Mallinson, D.E. Resasco, J. Catal. 281 (2011) 21–29.
- [23] D.E. Resasco, J. Phys. Chem. Lett. 2 (2011) 2294–2295.
- [24] D.J. Rensel, S. Rouvimov, M.E. Gin, J.C. Hicks, J. Catal. 305 (2013) 256–263.
- [25] H.H. Kung, Surface coordination unsaturation, in: Transition Metal Oxides: Surface Chemistry and Catalysis, Elsevier, Amsterdam, 1989.
- [26] P.M. Mortensen, J.-D. Grunwaldt, P.A. Jensen, A.D. Jensen, ACS Catal. 3 (2013) 1774–1785.
- [27] T. Prasomsri, T. Nimmanwudipong, Y. Roman-Leshkov, Energy Environ. Sci. 6 (2013) 1732–1738.
- [28] K. Leiva, N. Martinez, C. Sepulveda, R. García, C.A. Jiménez, D. Laurenti, M. Vrinat, C. Geantet, J.L.G. Fierro, I.T. Ghampson, N. Escalona, Appl. Catal. B 490 (2015) 71–79.
- [29] S. Koso, H. Watanabe, K. Okumura, Y. Nakagawa, K. Tomishige, Appl. Catal. B 111–112 (2012) 27–37.
- [30] S. Koso, Y. Nakagawa, K. Tomishige, J. Catal. 280 (2011) 221–229.
- [31] Y. Amada, Y. Shinmi, S. Koso, T. Kubota, Y. Nakagawa, K. Tomishige, Appl. Catal. B 105 (2011) 117–127.

- [32] S. Koso, N. Ueda, Y. Shinmi, K. Okumura, T. Kizuka, K. Tomishige, *J. Catal.* 267 (2009) 89–92.
- [33] Y. Nakagawa, Y. Shinmi, S. Koso, K. Tomishige, *J. Catal.* 272 (2010) 191–194.
- [34] K.-I. Shimizu, S. Kanno, K. Kon, *Green Chem.* 16 (2014) 3899–3903.
- [35] N. Ota, M. Tamura, Y. Nakagawa, K. Okumura, K. Tomishige, *Angew. Chem. Int. Ed. Engl.* 54 (2015) 1897–1900.
- [36] J. Yang, S. Li, L. Zhang, X. Liu, J. Wang, X. Pan, N. Li, A. Wang, Y. Cong, X. Wang, T. Zhang, *Appl. Catal. B* 201 (2017) 266–277.
- [37] Y.-K. Hong, D.-W. Lee, H.-J. Eom, K.-Y. Lee, *Appl. Catal. B* 150–151 (2014) 438–445.
- [38] S. Echeandia, P.L. Arias, V.L. Barrio, B. Pawelec, J.L.G. Fierro, *Appl. Catal. B* 101 (2010) 1–12.
- [39] L. Nie, P.M. de Souza, F.B. Noronha, W. An, T. Sooknoi, D.E. Resasco, *J. Mol. Catal. A: Chem.* 388–389 (2014) 47–55.
- [40] I.T. Ghompson, C. Sepulveda, A.B. Dongil, G. Pecchi, R. Garcia, J.L.G. Fierro, N. Escalona, *Catal. Sci. Technol.* 6 (2016) 7289–7306.
- [41] C.D. Wagner, L.E. Davis, M.V. Zeller, J.A. Taylor, R.H. Raymond, L.H. Gale, *Surf. Interface Anal.* 3 (1981) 211–225.
- [42] R.C. Nelson, B. Baek, P. Ruiz, B. Goundie, A. Brooks, M.C. Wheeler, B.G. Frederick, L.C. Grabow, R.N. Austin, *ACS Catal.* 5 (2015) 6509–6523.
- [43] M.B. Griffin, G.A. Ferguson, D.A. Ruddy, M.J. Biddy, G.T. Beckham, J.A. Schaidle, *ACS Catal.* 6 (2016) 2715–2727.
- [44] C. Newman, X. Zhou, B. Goundie, I.T. Ghompson, R.A. Pollock, Z. Ross, M.C. Wheeler, R.W. Meulenbergh, R.N. Austin, B.G. Frederick, *Appl. Catal. A* 477 (2014) 64–74.
- [45] P.M. Mortensen, J.D. Grunwaldt, P.A. Jensen, K.G. Knudsen, A.D. Jensen, *Appl. Catal. A* 407 (2011) 1–19.
- [46] A. Aqsha, L. Katta, N. Mahinpey, *Catal. Lett.* 145 (2015) 1351–1363.
- [47] S.R. Bare, S.D. Kelly, F.D. Vila, E. Boldingh, E. Karapetrova, J. Kas, G.E. Mickelson, F.S. Modica, N. Yang, J.J. Rehr, *J. Phys. Chem. C* 115 (2011) 5740–5755.
- [48] I.T. Ghompson, C. Sepulveda, R. Garcia, J.L.G. Fierro, N. Escalona, *Catal. Sci. Technol.* 6 (2016) 4356–4369.
- [49] I.E. Wachs, *Catal. Today* 27 (1996) 437–455.
- [50] K. Bhattacharyya, J. Majeed, K.K. Dey, P. Ayyub, A.K. Tyagi, S.R. Bharadwaj, *J. Phys. Chem. C* 118 (2014) 15946–15962.
- [51] M. Castriota, E. Cazzanelli, G. Das, R. Kalendarev, A. Kuzmin, S. Marino, G. Mariotto, J. Purans, N. Scaramuzza, *Mol. Cryst. Liq. Cryst.* 474 (2007) 1–15.
- [52] C.A. Majid, M.A. Hussain, *J. Phys. Chem. Solids* 56 (1995) 255–259.
- [53] B.D. Cullity, *Elements of X-ray Diffraction*, Addison-Wesley, London, 1978.
- [54] C. Zhao, Y. Yu, A. Jentys, J.A. Lercher, *Appl. Catal. B* 132–133 (2013) 282–292.
- [55] A.N. Desikan, L. Huang, S.T. Oyama, *J. Phys. Chem.* 95 (1991) 10050–10056.
- [56] I.E. Wachs, B.M. Weckhuysen, *Appl. Catal. A* 157 (1997) 67–90.
- [57] J. Haber, A. Kozlowska, R. Kozłowski, *J. Catal.* 102 (1986) 52–63.
- [58] M.G. Stachioni, F. Cor'a, C.R.A. Catlow, C.O. Rodriguez, *Phys. Rev. B* 55 (1997) 7508–7514.
- [59] K. Nakamoto, *Infrared and Raman Spectra of Inorganic and Coordination Compounds*, 6th ed., John Wiley & Sons, Inc., Hoboken, NJ, 2009.
- [60] L. Feng, X. Li, D.B. Dadyburjor, E.L. Kugler, *J. Catal.* 190 (2000) 1–13.
- [61] K.V.R. Chary, G. Kishan, T. Bhaskar, C. Sivaraj, *J. Phys. Chem. B* 102 (1998) 6792–6798.
- [62] F. Arena, N. Giordano, A. Parmaliana, *J. Catal.* 167 (1997) 66–76.
- [63] A.M. Abdel-Mageed, D. Widmann, S.E. Olesen, I. Chorkendorff, J. Biskupek, R.J. Behm, *ACS Catal.* 5 (2015) 6753–6763.
- [64] J. Chang, T. Danuthai, S. Dewiyanti, C. Wang, A. Borgna, *ChemCatChem* 5 (2013) 3041–3049.
- [65] A.M. de Jong, H.J. Borg, L.J. van IJzendoorn, V.G.F.M. Soudant, V.H.J. de Beer, J.A.R. van Veen, J.W. Niemantsverdriet, *J. Phys. Chem.* 97 (1993) 6477–6483.
- [66] K.V.R. Chary, T. Bhaskar, G. Kishan, V. Vijayakumar, *J. Phys. Chem. B* 102 (1998) 3936–3940.
- [67] J. Okal, W. Tylus, L. Kępiński, *J. Catal.* 225 (2004) 498–509.
- [68] C.D. Wagner, W.M. Riggs, L.E. Davis, J.F. Moulder, *Handbook of X-ray Photoelectron Spectroscopy*, Perkin-Elmer Corporation, Eden Prairie, MN, 1979.
- [69] E. Hryha, E. Rutqvist, L. Nyborg, *Surf. Interface Anal.* 44 (2012) 1022–1025.
- [70] M. Ferrari, B. Delmon, P. Grange, *Carbon* 40 (2002) 497–511.
- [71] Y. Shinmi, S. Koso, T. Kubota, Y. Nakagawa, K. Tomishige, *Appl. Catal. B* 94 (2010) 318–326.
- [72] N. Boufaden, R. Akbari, B. Pawelec, J.L.G. Fierro, M.S. Zina, A. Ghorbel, *J. Mol. Catal. A: Chem.* 420 (2016) 96–106.
- [73] K.H. Kang, U.G. Hong, Y. Bang, J.H. Choi, J.K. Kim, J.K. Lee, S.J. Han, I.K. Song, *Appl. Catal. A* 490 (2015) 153–162.
- [74] C. Hoang-Van, O. Zegaoui, *Appl. Catal. A* 130 (1995) 89–103.
- [75] M.A.P. da Silva, M. Schmal, *Catal. Today* 85 (2003) 31–37.
- [76] J.T. Miller, B.L. Meyers, M.K. Barr, F.S. Modica, D.C. Koningsberger, *J. Catal.* 159 (1996) 41–49.
- [77] R. Navia, B. Pawelec, P. Castaño, M.C. Álvarez-Galván, C.V. Loricera, J.L.G. Fierro, *Appl. Catal. B* 92 (2009) 154–167.
- [78] K.I. Hadjiivanov, D.G. Klissurski, A.A. Davydov, *J. Catal.* 116 (1989) 498–505.
- [79] G. Bagnasco, *J. Catal.* 159 (1996) 249–252.
- [80] H. Idriss, M.A. Bartea, *Adv. Catal.*, in: H.K. Bruce, C. Gates (Eds.), Academic Press, 2000, pp. 261–331.
- [81] Y.R. Luo, *Comprehensive Handbook of Chemical Bond Energies*, CRC Press, Taylor & Francis Group, Boca Raton, FL, 2007.
- [82] G. Liu, Z.-J. Zhao, T. Wu, L. Zeng, J. Gong, *ACS Catal.* 6 (2016) 5207–5214.
- [83] M. Huuska, J. Rintala, *J. Catal.* 94 (1985) 230–238.
- [84] Y.I. Yermakov, B.N. Kuznetsov, Y.A. Ryndin, *J. Catal.* 42 (1976) 73–78.